https://doi.org/10.5194/egusphere-2025-5359
Preprint. Discussion started: 5 February 2026

LOAC-OCB v1.0: A model to explore terrestrial organic carbon burial along the land-to-ocean aquatic continuum

Daniela Henry-Pinilla[1], Núria Catalán[1], Biel Obrador[2], and Rafael Marcé[1]

[1]Centre d'Estudis Avançats de Blanes (CEAB-CSIC), Accès a la Cala Sant Francesc 14, Blanes, 17300, Catalonia, Spain
[2]Universitat de Barcelona, Departament de Biologia Evolutiva, Ecologia i Ciències Ambientals, Institut de Recerca de la Biodiversitat, Avenida Diagonal 643, Barcelona, 08028, Catalonia, Spain

Correspondence: Daniela Henry-Pinilla (daniela.henry@ceab.csic.es)

Abstract. Various aquatic environments along the land-to-ocean aquatic continuum (LOAC) retain and potentially bury significant amounts of organic carbon (OC). However, the total amount of buried OC, the relative importance of different ecosystems in this process, and the hierarchical influence of upstream systems on downstream burial dynamics remain uncertain. A major limitation in quantifying these processes is the absence of an integrative, process-based modeling framework operating at Earth system scales. Here, we present the LOAC-OCB model, the first global tool for simulating the transport and burial of particulate terrestrial OC along the LOAC. Using openly available data products, this steady-state model provides spatially explicit organic carbon burial (OCB) estimates at 0.0625 x 0.0625º spatial scale, incorporating 170,997 lakes, 6,000 reservoirs, 3,515 floodplains, and 377 coastal ecosystems worldwide. The model was evaluated through a multi-faceted validation using independent global datasets and previously published estimates. Our results indicate that the LOAC buries approximately 52.1% of the particulate OC imported from terrestrial ecosystems, with reservoirs and coastal ecosystems showing the highest median OCB rates (94.3 $\pm$ 3.8 and 53.1 $\pm$ 14.1 g C m^{-2} y^{-1}, respectively). Additionally, floodplains and reservoirs exert the greatest influence on global OCB fluxes, contributing 0.97 and 0.72 Pg C y^{-1}, respectively. LOAC-OCB also enables further exploration of the interactions among aquatic ecosystems, shedding light on their interconnected roles in the global distribution of OCB and the relevance of burial processes in modulating terrestrial-to-ocean OC fluxes.

1 Introduction

Understanding how carbon (C) is redistributed among Earth's major compartments is critical not only for constraining the global C budget and tackling climate change (Friedlingstein et al., 2022; Regnier et al., 2022; Webb et al., 2019), but also for assessing the growing influence of human activities such as dam construction (Maavara et al., 2017) and the deforestation of coastal habitats (Lovelock and Reef, 2020; Rosentreter et al., 2023). Continental aquatic ecosystems play a key role in this redistribution, mediating both the lateral transport of C from land to ocean and the long-term burial of C in sediments along the land-to-ocean aquatic continuum (LOAC) (Kirwan et al., 2023; Lininger and Wohl, 2019; Mendonça et al., 2017).

Recent studies estimate that approximately 5.1 Pg C y^{-1} are exported from soils to river networks (Drake et al., 2018), while only 1.02 $\pm$ 0.22 Pg C y^{-1} ultimately reaches the ocean via river mouths (Liu et al., 2024). This suggests that nearly 4 Pg C y^{-1} are mineralized and emitted to the atmosphere, or buried in inland and coastal sediments (i.e., within the LOAC). A large

https://doi.org/10.5194/egusphere-2025-5359
Preprint. Discussion started: 5 February 2026

fraction of this C transported along the LOAC is in the form of organic carbon (OC) (Aufdenkampe et al., 2011; Battin et al., 2009; Regnier et al., 2022). It has been estimated that about 40% of the total C transported by riverine systems to the ocean is OC (Tamooh et al., 2012), and a substantial portion of this OC (0.43 Pg C y^{-1}, Schlünz and Schneider (2000)) is of terrigenous origin (allochthonous from the point of view of LOAC ecosystems), derived from soils and vegetation in upstream terrestrial environments (Drake et al., 2018). This terrestrial input is especially dominant in systems such as small lakes with short water residence times, lakes with large watershed areas, or catchments subject to intense erosion (Mulholland and Elwood, 1982). Compared to autochthonous OC produced within aquatic systems, terrestrial OC tends to be more persistent and less available to microbial degradation (Guillemette et al., 2013; Kothawala et al., 2021), which increases its likelihood of long-term burial (Sobek et al., 2009).

In addition to its origin and reactivity, the form of OC also influences its fate. Particulate organic carbon (POC) is frequently the most abundant C pool being transported by riverine systems (Beusen et al., 2005). Moreover, due to its greater size and density, POC is more likely to settle than DOC. Although DOC may flocculate or adsorb to mineral surfaces under certain conditions, terrestrial POC is intrinsically more susceptible to sedimentation (Li et al., 2024). Combined with its lower reactivity relative to autochthonous OC, this makes allochthonous POC a dominant contributor to organic carbon burial (OCB) in depositional environments (Gudasz et al., 2017). Recent estimates suggest that approximately 0.55 $\pm$ 0.25 Pg OC y^{-1} are buried in continental aquatic ecosystems alone (Regnier et al., 2022), highlighting their global relevance as long-term C sinks.

However, great uncertainty persists in current global C budget assessments, particularly regarding the LOAC's contribution to OCB. Current studies report uncertainties of 50% - 100%, largely due to limited understanding of lateral C fluxes (Regnier et al., 2022). In addition, Drake et al. (2018) determines that there is high uncertainty of C burial in inland waters, noting that this uncertainty strongly affects global estimations of terrestrial C transport. Numerous studies have provided comprehensive estimations for OCB within individual ecosystem types, such as coastal ecosystems (Breithaupt et al., 2012; Ouyang and Lee, 2014; Serrano et al., 2016), lakes (Anderson et al., 2014; Dietz et al., 2015; Heathcote et al., 2015; Kortelainen et al., 2013), reservoirs (Luo et al., 2016; Mendonça et al., 2017; Pittman et al., 2013), floodplains (Noe and Hupp, 2009; Sanders et al., 2017; Walling et al., 2006) or other types of wetlands (Bernal and Mitsch, 2013). These ecosystem-specific studies have demonstrated the relevance of these environments as OC sinks, improved understanding of OC dynamics and burial mechanisms, and provided estimates of OCB rates that serve as valuable inputs for validating large-scale models.

Nevertheless, only a few global C models have incorporated OCB, and none has integrated burial across the various ecosystem types of the LOAC (Henry et al., 2024). This lack of integration is critical, as it may obscure large-scale C dynamics along the LOAC. For instance, reservoirs have substantially altered global OCB patterns by trapping sediments (Mendonça et al., 2017) and OC that would otherwise be transported downstream, emitted to the atmosphere, or buried in other ecosystems. However, without a comprehensive understanding of the fate of POC before and after dam construction the net effect of this anthropogenic alteration remains uncertain, raising questions about whether reservoirs enhance global OCB or merely redistribute it across ecosystems.

Previous global models have typically focused on individual environments or partial segments of the LOAC and if they represent sedimentation and burial, it is done often in an implicit way. For instance, models such as Global NEWS2 (Mayorga

https://doi.org/10.5194/egusphere-2025-5359
Preprint. Discussion started: 5 February 2026

et al., 2010), INCA-C (Futter et al., 2007), and ORCHILEAK (Gommet et al., 2022) simulate lateral C transport but do not explicitly resolve sedimentation or OCB, while DLEM2.0 (Tian et al., 2015) includes POC deposition but do not account for burial. Maavara et al. (2017) estimate OCB using a mass-balance approach, whereas TRIPLEX-HYDRA (Li et al., 2022) considers POC trapping in reservoirs but does not simulate its interaction with downstream ecosystems. ROMS-NENA (Druon et al., 2010), in contrast, explicitly accounts for POM resuspension and POC burial on continental margins, with resuspension modeled as a function of bottom friction velocity and burial efficiency proportional to sedimentation. However, unlike the other models, ROMS-NENA does not include lateral transport from inland systems and focuses solely on coastal C dynamics. As a result, none of these models captures how C processes in one ecosystem influence processes and fluxes in another, limiting their ability to represent the integrated functioning of the LOAC.

A key knowledge gap therefore remains in understanding the spatial distribution of terrestrial OC burial across the diverse ecosystems of the LOAC and the extent to which they are interconnected (Henry et al., 2024). An integrated perspective is needed to quantify how OC flows through and is buried within the LOAC, from headwater streams to coastal margins. Such integration is essential to improve global C budgets, identify key C sinks, understand the relative importance of different C pathways, and assess the influence of human activities on C dynamics at both regional and global scales (Regnier et al., 2022). Developing models that encompass the key LOAC components is thus a pressing need to capture the complexity of inland-to-coastal OC transport and burial.

In this study, we present LOAC-OCB, the first global model that simulates OCB of terrestrial POC across the entire LOAC within a unified, process-based framework. The model integrates lakes, reservoirs, floodplains, and coastal systems to provide a consistent representation of sedimentation, mineralization, and burial processes along the aquatic continuum. This integrative approach enables, for the first time, a comprehensive assessment of how terrestrial POC is distributed and buried across interconnected aquatic ecosystems at a global scale. Our goal is to offer a modeling tool for evaluating the anthropogenic impacts on the global C budget and for informing future decision-making related to water infrastructure and ecosystem management.

2 Methods

2.1 Model description

The LOAC-OCB is a process-based, steady-state model developed to track the fate of terrestrial POC from its source in soils to its burial within LOAC ecosystems. It operates globally at a spatial resolution of 0.0625º x 0.0625º. For hydrological calculations, we consider that using mean runoff derived from ∼100 years of data provides a robust basis for simulating steady-state processes. Model outputs can be expressed as annual rates to facilitate comparisons with other modeling approaches and observational data. The model includes river networks and four main contrasting depositional environments: lakes, man-made reservoirs, river floodplains, and coastal blue-carbon ecosystems. LOAC-OCB, based on a mathematical graph structure (Zhang and Chartrand, 2006), is implemented in Python 3.8, primarily using the *gdal* (Rouault et al., 2023) and *networkx* (Hagberg et al., 2008) libraries for geospatial data manipulation and network-based routing. It is openly available and can be run and reproduced by using a virtual environment to execute Python scripts.

https://doi.org/10.5194/egusphere-2025-5359
Preprint. Discussion started: 5 February 2026

LOAC-OCB operates in three sequential steps. The first step establishes the hierarchy of the river network. The second step adds the depositional environments and their physical properties, i.e., water depth and temperature, and ecosystem area and volume. This step also generates runoff and discharge, which determines the routing of water and sediments along the river network. Together, the river topology, hydrology, and ecosystem properties allow for the calculation of water residence times. The third step executes the processes influencing the burial of POC along the LOAC, such as sediment generation, OC mineralization, sedimentation, and burial.

LOAC-OCB requires a range of input data provided as global raster maps. These include terrain characteristics (e.g., slope and flow direction), hydrological variables (e.g., runoff), and ecosystem properties (e.g., area, volume, depth and water temperature), sediment generation from soils, and soil properties such as OC content and the proportion of clay, silt and sand, as we assumed the generated sediments to conserve those properties from the original soils. A complete list of inputs is provided in Table 1 and further detailed in Section 2.5.

Model outputs include a raster file containing customizable variables and parameters, which may include, among others, sediment and OC inputs to aquatic ecosystems, sedimentation, OCB, OC export to the downstream network, and OC mineralization. All components of the sediment and OC mass balances for each ecosystem are accessible. Additionally, information such as ecosystem type, surface area, volume, depth, residence time, discharge, particle size fractions, and both retention and burial efficiencies can be obtained. A complete list of outputs is provided in the Annex, in Table B1-B6.

2.2 Model workflow and coding strategy

The **first step** builds a base graph, generating a network topology based on terrain slope and flow direction. A graph, in this context, is a mathematical structure consisting of nodes (representing spatial units) and edges (representing connections between them) (Zhang and Chartrand, 2006), used to represent a hierarchical flow network through which water and sediment will be routed (Fig. 1). The Python codes for the generation of the graph are based on Klink et al. (2024). The **second step** builds upon this structure by incorporating depositional environments, classified into four main types: lakes (natural lakes larger than 0.1 km^2), reservoirs (man-made impoundments), floodplains (regularly or seasonally flooded riverine and palustrine systems, both forested and non-forested), and coastal ecosystems (blue-carbon habitats such as mangroves, seagrasses, and salt marshes). Such classification is based on the different data sources used to identify each of these ecosystems (Table 1). Any node that is not classified as a depositional environment is classified as a *river* node. Hydrological attributes such as runoff, ecosystem area, volume, water depth, and temperature are also incorporated at this step, together with the computation of discharge and water residence time. In the **third step**, the model simulates core biogeochemical processes including OC mineralization, sedimentation, and burial. Sediment inputs from the soils to the LOAC are estimated based on erosion induced by water displacement, while the OC content is derived from the soil organic carbon of the contributing area. These sediments enter the depositional environments with their associated OC content and may undergo sedimentation and burial, mineralization, or be exported downstream. The script structure reflects this three-step workflow and is modular by design, facilitating user comprehension, modification, and extension (e.g., expanding the model framework or integrating additional modules).

https://doi.org/10.5194/egusphere-2025-5359
Preprint. Discussion started: 5 February 2026

Within the graph structure, nodes play distinct roles (Figs. 1 and 2). Each node is represented by a single raster cell at the model's defined spatial resolution. At the working spatial resolution, all nodes in the graph conceptually represent both a portion of land and the embedded river network that routes water and sediments, both generated locally in the node and coming from upstream nodes (i.e., *parent* nodes). The inclusion of specific aquatic ecosystems is achieved by rasterizing available products on the global distribution of lakes, reservoirs, floodplains, and coastal ecosystems. Each depositional aquatic ecosystem is represented by a single *burial* node, which is the most downstream node of the ecosystem and stores aggregated properties of the entire ecosystem (e.g., area, volume, depth). The *burial* node is where sedimentation, OC mineralization, and OCB are calculated. This node also represents the ecosystem's outlet. In coastal systems, where all nodes are equally downstream, one of those is designated as the *burial* node (Fig. 1). Other nodes within the same depositional aquatic ecosystem, if any, are treated as *dummy* nodes. These nodes route water and sediments to the *burial* node but do not simulate any biogeochemical processing. We coded the ecosystem nodes in this way (differentiating *burial* and *dummy* nodes) because the steady-state nature of the model that assumes equilibrium using annual hydrological variables would make modeling internal heterogeneity within single ecosystems disputable. All other nodes outside of depositional systems function as *river* nodes, where only OC mineralization occur, reducing the OC load during transit. This implies that river channels, over the long-term, are not considered as depositional environments. Instead, floodplains are incorporated to account for burial not associated to lakes and reservoirs.

At each step of the model, users can modify parameters. In the initial section of each script, users can also define a different spatial extent for the graph to be generated and, thus of the final raster outputs. This extent must be equal to or smaller than that of the original input rasters and should be specified in degree coordinates (CRS: WGS 84). Furthermore, users can adjust several parameters and choose which output files to generate, their formats, and their naming conventions.

2.3 Processes

Beyond water transport, the key processes determining the distribution of POC along the LOAC include sediment generation and transport, suspended solids sedimentation, and OCB. OC mineralization occurs in both *river* and *burial* nodes, accounting for OC loss during transit and at depositional sites. In contrast, sedimentation of suspended solids and OCB are restricted to *burial* nodes, where depositional conditions allow for long-term carbon burial (Fig. 2).

2.3.1 Sediment generation

Terrestrial POC export is mostly controlled by physical erosion (Galy et al., 2015). In the LOAC-OCB model, sediment loads transported and processed along the LOAC originate from soil erosion and subsequent displacement by water. This process is represented at all node types using an erosion rate, expressed in Mg ha^{-1} yr^{-1}, which is input as a raster map. Sediment loads are further partitioned into three particle size fractions, i.e., clay, silt, and sand, since particle size strongly influences settling velocity (Ahrens, 2003). The sediment mass balance at each node is calculated separately for each fraction and then summed to obtain the total sediment input and export loads.

https://doi.org/10.5194/egusphere-2025-5359
Preprint. Discussion started: 5 February 2026

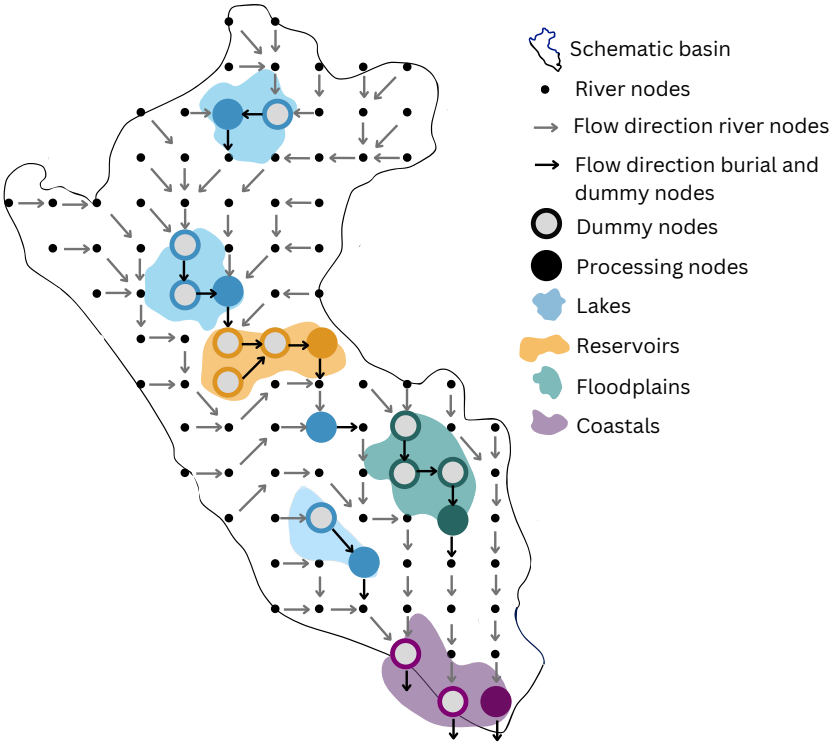

Figure 1. Conceptual diagram of a schematic basin showing how the model's node types (i.e. river, dummy, and burial) are spatially connected. Aquatic ecosystems are represented using distinct colors, which are used consistently in subsequent figures.

2.3.2 Sedimentation

Once particulate sediments reach *burial* nodes, they are subject to sedimentation as suspended particulate matter. Sedimentation is defined as the vertical flux of suspended particulate matter during a certain period of time, and therefore expressed as a rate with units of mass per time. In our model, we do not solve for gross sedimentation and sediment resuspension separately, therefore sedimentation rates account for net sedimentation (Henry et al., 2024), which we refer to simply as sedimentation from here on.

Sedimentation rates are estimated by calculating a sediment trapping efficiency (TE, expressed in $\%$) for each ecosystem and multiplying it by the incoming sediment load:

$$SED_{\text{depo}} = SED_{\text{input}} \cdot TE, \tag{1}$$

where SED_{depo} is the sedimentation rate (kg y^{-1}); and SED_{input} is the total incoming sediment load (kg y^{-1}), including local generation and contribution from the *parent* nodes. The pool of deposited sediments, defined as the accumulation of particles due to sedimentation, is assumed to have the same OC content as the sediments entering the node. This pool can either be permanently buried or undergo mineralization, releasing OC back into the water column.

https://doi.org/10.5194/egusphere-2025-5359
Preprint. Discussion started: 5 February 2026

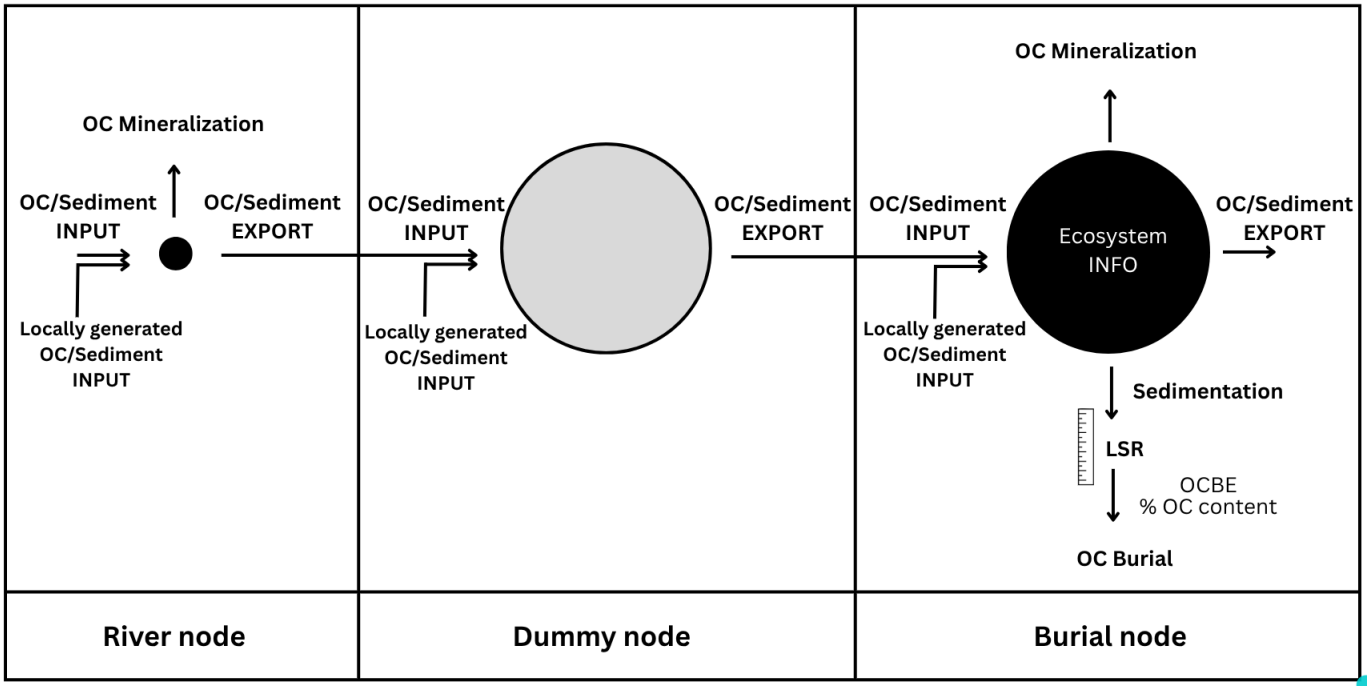

Figure 2. Main structural and functional distinctions between the node types used in the LOAC-OCB model. OC: organic carbon; LSR: linear sedimentation rate; OCBE: organic carbon burial efficiency. Parent nodes refer to upstream nodes, regardless of their type.

2.3.3 Burial

Organic carbon burial (OCB) represents the fraction of sedimented OC that becomes permanently stored within aquatic sediments due to negligible decomposition and stable environmental conditions (Henry et al., 2024). OCB is reported either as an areal rate (OC_{bur}, in g C m^{-2} y^{-1}) or as a whole-system rate (OC_{bur-ws}, in g C y^{-1}). OCB is calculated using a unified approach across all ecosystem types. As with sedimentation, OCB is only calculated in *burial* nodes, but considering the total ecosystem area and volume—that is, the sum of the *burial* and its associated *dummy* nodes, if any (Fig. 2). The whole-system burial rate, $OC_{\mathrm{bur-ws}}$, is computed as:

$$OC_{\mathrm{bur-ws}} = OC_{\mathrm{depo}} \cdot OCBE/100. \quad (2)$$

Here, OC_{depo} is the OC content of the deposited sediment ($SED_{\mathrm{depo}} \cdot \%OC_{\mathrm{depo}} \cdot 1000$, expressed in g C y^{-1}); and $OCBE$ is the burial efficiency (%), reflecting the fraction of OC_{depo} that is effectively buried over the long-term.

2.3.4 Mineralization

The total OC mineralization ($OC_{\mathrm{min-total}}$, in g C y^{-1}), defined as the decomposition of OC into carbon dioxide (CO_2) and methane (CH_4), occurs in both *burial* and *river* nodes (Fig. 2). At each node, $OC_{\mathrm{min-total}}$ is the sum of two components:

https://doi.org/10.5194/egusphere-2025-5359
Preprint. Discussion started: 5 February 2026

OC_{min} and $OC_{\mathrm{min-sed}}$. The first component (OC_{min}, in g C y^{-1})) accounts for mineralization in water and is calculated using a first-order exponential decay model applied to the portion of OC input that is not sedimented:

$$OC_{\mathrm{min}} = (OC_{\mathrm{input}} - OC_{\mathrm{depo}}) \cdot (1 - \exp(-k_{20} \cdot \theta^{T_{\mathrm{w}}^{\circ}-20}) \cdot RT). \quad (3)$$

In this equation, OC_{input} represents the total input of OC (g C y^{-1}); k_{20} is the mineralization rate at 20ºC (d^{-1}); θ is a dimensionless temperature correction coefficient; RT is the water residence time (d), and T_w° is the mean annual water temperature (C). The second component ($OC_{\mathrm{min-sed}}$, in g C y^{-1}) represents mineralization within the sediments and is derived from the mass balance between deposited OC and buried OC (Eq. 4), assuming that any OC deposited but not buried is eventually mineralized:

$$OC_{\mathrm{min-sed}} = OC_{\mathrm{depo}} - OC_{\mathrm{bur-ws}}. \quad (4)$$

2.4 Model parameterization

For each ecosystem type, we reviewed methodologies previously used in the literature, evaluated available tools and approaches for parameterization, and identified suitable data sources to extract or derive the necessary model parameters. A summary of the parameterization of LOAC-OCB variables is provided in Tables B1-B7 in the Annex.

2.4.1 Ecosystem area

The areas of lakes and reservoirs are directly extracted from HydroLAKES (Section 2.5), which provides explicit surface area data for individual water bodies. This information is assigned to the corresponding *burial* node in the LOAC-OCB. For floodplains and coastal systems, surface area is estimated at their respective *burial* node by summing the ecosystem area stored in all nodes associated to the same ecosystem unit. The definition of these units is detailed in Section 2.5.

2.4.2 Water depth

Water depth estimates for lakes are extracted from the HydroLAKES database (Section 2.5). Water depth in *river* nodes is estimated using a discharge-based relationship derived from hydraulic geometry theory (Leopold and Maddock, 1953; Andreadis et al., 2013):

$$D_w = d \cdot q^e, \quad (5)$$

where D_w is the water depth (m), q is the discharge (m^3 s^{-1}), and d = 0.27 and e = 0.3 are dimensionless empirical constants. For floodplains, the depth used in model calculations corresponds to the difference in depth between maximum and mean discharge conditions, both estimated using Eq. 5. This relies on the assumption that floodplain depth reflects the additional water level associated with overbank flows, i.e., the increment in water depth generated by peak discharge events relative to baseflow conditions. In coastal systems, we assign representative mean depths based on ecosystem type: 1 m for mangroves and saltmarshes (Yang et al., 2012), and 15 m for seagrasses (Luhar et al., 2013). For coastal units containing more than one ecosystem type, a weighted mean depth is calculated based on the proportional area of each ecosystem present.

https://doi.org/10.5194/egusphere-2025-5359
Preprint. Discussion started: 5 February 2026

2.4.3 Residence time

In *river* nodes, residence time is estimated using Eq. 6, which depends on the node's discharge, slope and stream segment length, following the approach by Schulze et al. (2005):

$$RT = \frac{l}{n \cdot R^{2/3} \cdot s^{1/2}}, \tag{6}$$

where RT is the water residence time (s); l is the length of the stream segment (m) that depends on the flow direction; $n = 0.044$ is the Manning coefficient (s $m^{1/3}$) (Font et al., 2019); R is the hydraulic radius (m); and s the channel slope (m m^{-1}). For lakes, reservoirs, floodplains, and coastal ecosystems, RT is estimated as the ratio of water volume (i.e., ecosystem area (A_{system}) multiplied by D_w, in m^3) to discharge (q), assuming steady-state. In floodplains, RT is calculated using maximum discharge ($q = q_{\max}$) under the assumption that most sediment transport to floodplains and consequent sedimentation occurs under peak flow conditions (Section 2.5 for derivation of $q = q_{\max}$). In coastal systems, the discharge q represents the sum of all contributing nodes (both *dummy* and *burial* nodes) within the unit. This reflects the fact that although discharge occurs at multiple outlets, sedimentation and burial are computed only at the designated *burial* node for the coastal unit.

2.4.4 Trapping Efficiency

Three different approaches are used to determine sediment TE, depending on the ecosystem type.

Lakes and reservoirs: TE is calculated following the empirical asymptotic retention curves for clay (i.e., fine, Eq. 7), silt (i.e., medium, Eq. 8), and sand (i.e., coarse, Eq. 9) particles proposed by Gill (1979). In this approach, Gill combined the empirical trap efficiency relationships developed by Brune (1953) with a reservoir sedimentation model.

$$TE_{\text{clay}} = \frac{RT^3}{1.02655 \cdot RT^3 + 0.02621 \cdot RT^2 - 0.133 \cdot 10^{-3} \cdot RT + 0.1 \cdot 10^{-5}}, \tag{7}$$

$$TE_{\text{silt}} = \frac{RT}{0.012 + 1.02 \cdot RT}, \tag{8}$$

$$TE_{\text{sand}} = \frac{RT^2}{0.994701 \cdot RT^2 + 0.006297 \cdot RT + 0.3 \cdot 10^{-5}}, \tag{9}$$

with RT in y.

Floodplains: Sediment TE in floodplains remains poorly characterized at the global scale. Representing floodplain sediment dynamics is particularly challenging due to their complex hydrology and morphology. These systems are highly dynamic, with erosion, deposition, and transport processes occurring simultaneously across different sections of the river, continuously reshaping the landscape over both short and long timescales (Geyman et al., 2025). While some models have successfully captured these complexities (Greenberg et al., 2024; Torres et al., 2017), they have not yet been applied to estimate sediment retention or OCB at the global scale. Noe and Hupp (2009) estimated sediment trapping efficiency across multiple freshwater coastal riverine floodplains, reporting values between 23 and 87% sediment retention, with a median of 54%, irrespective of particle size. Based on this study, we adopted a fixed TE value of 0.54 (i.e., 54% of incoming sediment is retained).

https://doi.org/10.5194/egusphere-2025-5359
Preprint. Discussion started: 5 February 2026

Coastal ecosystems: In coastal systems, TE is calculated using a negative exponential model (Eq. 10), which takes into consideration that slower velocities, shorter residence times and deeper water columns will diminish the proportion of sediments that ultimately accumulates at the bottom of the water body. The equation is as follows (Chen, 1975):

$$TE = 1 - \exp\left(-RT \cdot \frac{v}{D_w}\right), \tag{10}$$

with RT in s. v is the particle velocity (m s^{-1}), calculated using the method proposed by Ahrens (2003) to estimate fall velocity for each particle size fraction. v/D_w represents the inverse of the particle's settling time (s^{-1}). This formulation is adapted from the Archimedes buoyancy index and accounts for particle size–dependent settling behavior. Distinct particle radii were assigned to each sediment class following Hatono and Yoshimura (2020): 1×10^{-6} m for clay, 2.5×10^{-5} m for silt, and 1×10^{-3} m for sand.

2.4.5 OCB

To estimate burial at *burial* nodes, we developed an empirical sigmoidal relationship between linear sedimentation rate (LSR, mm y^{-1}) and OCBE (Eq. 13, Fig. 3). LSR represents the depth of sediments accumulating at the bottom of a water body over time, while OCBE is the quotient between OCB and OC sedimentation (Henry et al., 2024). Although this relationship has been documented in depositional marine systems (Betts and Holland, 1991; Ingall and Cappellen, 1990; Katsev and Crowe, 2015), it has not, to the best of our knowledge, been systematically explored in freshwater environments, nor applied in Earth System Models. For freshwater systems, the sigmoidal curve is derived from 30 observational data points across 13 lakes and reservoirs (Henry et al., 2024). Due to the limited availability of data for floodplains and acknowledging that their inherent complexity may not be fully represented, we assumed that their sediment–OC dynamics resemble those of other freshwater depositional environments, applying the same sigmoidal relationship. For coastal systems, the curve is adjusted to reproduce a relationship consistent with that reported by Katsev and Crowe (2015) for marine environments.

In LOAC-OCB, LSR and $OCBE$ are determined through an iterative process, ensuring the sediment and OC mass balances are maintained after sedimentation, burial, and mineralization are computed at each *burial* node. The model assumes that all sedimented OC is either buried or mineralized. The first iteration starts with the assumption that the sediment burial rate (SED_{bur}, in kg C m^{-2} y^{-1}) and its OC content ($\%OC_{\mathrm{bur}}$) are equal to SED_{depo} and $\%OC_{\mathrm{depo}}$, respectively. Using these initial values, LSR (Eq. 11) and $OCBE$ (Eq. 13) are calculated:

$$LSR = \frac{SED_{\mathrm{bur}}}{DBD}, \tag{11}$$

where DBD is the dry bulk density in g cm^{-3}, estimated following Keogh et al. (2021):

$$DBD = \frac{\alpha}{1 + \alpha \cdot \beta \cdot \%OC_{\mathrm{bur}} \cdot 2}. \tag{12}$$

with α = 2.296 and β = 0.139. $OCBE$ is then obtained from LSR using the above-mentioned sigmoidal fit:

$$OCBE = \frac{100}{1 + \exp(-b \cdot (ln(LSR) - c))}, \tag{13}$$

https://doi.org/10.5194/egusphere-2025-5359
Preprint. Discussion started: 5 February 2026

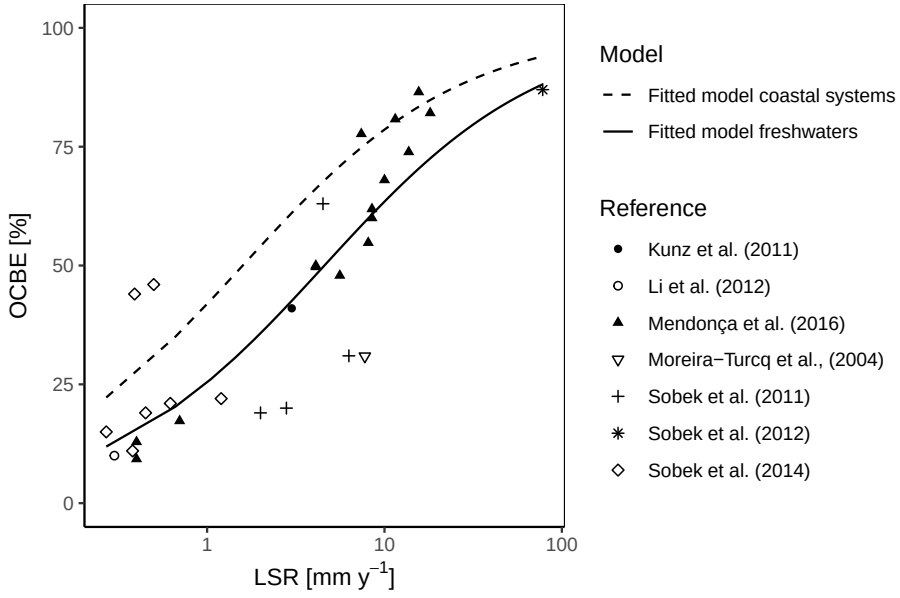

Figure 3. Sigmoidal relationship between organic carbon burial efficiency (OCBE, in %) and linear sedimentation rate (LSR, in mm y^{-1}) derived from 30 observational data points across 13 lakes and reservoirs. Symbols indicate different data sources. The solid curve represents the empirical model fitted to freshwater observational data by Henry et al. (2024), with parameters b = 0.7068 and c = -0.78 (Eq. 13), and is applied to lakes, reservoirs and floodplains. The dotted curve is an adjusted version of the same model, with c = –1.84, modified to reproduce a similar relationship reported by Katsev and Crowe (2015) for marine systems (not shown in this figure), and is used for coastal systems.

where b and c are parameters fitted to the freshwater or marine datasets (Fig. 3). With $OCBE$, Eq. 2 yields $OC_{\mathrm{bur-ws}}$ or OC_{bur}, the latter obtained by dividing OC_{bur-ws} by A_{system} (m^2). Then, the OC content of buried sediments is refined by recalculating the sediment burial pool (Eq. 14), which was initially assumed to equal the deposited sediments, to ensure sediment mass balance:

$$SED_{\mathrm{bur}} = OC_{\mathrm{depo}} - OC_{\mathrm{min-sed}}, \tag{14}$$

$$\%OC_{\mathrm{bur}} = OC_{\mathrm{ws}} \cdot 100 / SED_{\mathrm{bur}}. \tag{15}$$

The process iterates until $\%OC_{\mathrm{bur}}$ stabilizes, defined as a change of less than 0.001 % between iterations. Convergence typically occurs before 15 iterations, after which a final calculation of DBD, SED_{bur}, LSR, and $OCBE$ is performed to produce the final values.

2.4.6 k_{20} and θ

In the model, k_{20} is the OC mineralization rate at 20ºC (d^{-1}), calculated following Catalán et al. (2016):

$$k_{20} = \kappa \cdot RT^{-\eta}, \tag{16}$$

https://doi.org/10.5194/egusphere-2025-5359
Preprint. Discussion started: 5 February 2026

with RT in d, $\kappa = 0.0147$, and $\eta = 0.448$.

The temperature correction coefficient, θ, is a dimensionless parameter accounting for the temperature dependency of OC mineralization and is set to 1.07 following Maavara et al. (2017).

2.4.7 Water temperature

For *river* and coastal *burial* nodes, the model uses yearly mean river temperatures, while for lakes, reservoirs and floodplains, yearly mean bottom lake temperatures are applied.

2.5 Input data

Input data are obtained from diverse global sources (Table 1). These global products are openly available and are mostly derived from other models, remote sensing, or large databases. All inputs are adapted and unified to common spatial resolution and raster file format (TIFF). This first version of LOAC-OCB was globally validated at a spatial resolution of 0.0625º x 0.0625º. Inputs are incorporated into the model in the different steps, depending on their relevance to each stage of the modeling process.

2.5.1 Inputs step 1

In the first step, only the flow direction and slope rasters are incorporated. These datasets define the topological ordering of nodes and establish the structure of the river network. The rasters are obtained from (Font et al., 2019), produced at the same spatial resolution used in this model. The original flow direction data are derived from digital elevation models produced by HydroSHEDS (Lehner et al., 2008) and Hydro1k (VERDIN, 2011), while the slope data is derived from the Dominant River Tracing database (Wu et al., 2012).

2.5.2 Inputs step 2

In the second step, depositional aquatic ecosystems and their physical properties are incorporated into the model. Their allocation across the river network, and the assignment of their attributes (i.e surface area, volume, and depth), are performed using different methodologies to account for heterogeneity in data format and spatial scale among available sources. Locations and attributes of lakes and reservoirs are sourced from HydroLAKES (Messager et al., 2016) and rasterized to a 0.0625º x 0.0625º spatial resolution. The HydroLAKES database contains approximately 1.4 million water bodies, and at the model's spatial resolution, multiple systems may occur within the same pixel. To address this, we selected a single representative water body per pixel, adapting the methodology used by the ISIMIP Lake Sector (Golub et al., 2022) to the spatial resolution of this study. Lakes identified as isolated from the river network by Sikder et al. (2023) are excluded, as our focus is on depositional environments that are part of the LOAC and may contribute to sediment and OC transport. Given that lakes vastly outnumber reservoirs, and to maintain adequate representation of reservoir systems globally, reservoirs are given priority when both systems occur within a pixel.

https://doi.org/10.5194/egusphere-2025-5359
Preprint. Discussion started: 5 February 2026

This version of LOAC-OCB considers one representative lake or reservoir per node and, conceptually, assumes that it is located along the main river channel, since each node receives all upstream runoff as a single unit. Although the model operates at a relatively fine spatial resolution and isolated systems are already excluded, some potential mismatches in discharge assignment can still occur due to the working spatial scale. For instance, a reservoir or lake may be located at a tributary near the confluence with the main channel, but not in the main channel itself, which would be the assumption of the graph if the water body is so close to the confluence that it lies within the same pixel as the confluence itself. This kind of misalignment creates artifacts where an ecosystem can receive much bigger inputs than in reality if the tributary ends up in a comparatively very large river. To avoid this kind of spatial mismatches, we explored the discrepancies between the catchment area for each system reported in HYDROLAKES and the catchment areas calculated by adding up the areas of all upstream nodes in the graph. Then, we decided to exclude all lakes and reservoirs for which modeled catchment area with the graph differed by more than one order of magnitude from the reference dataset. After this filtering and the previous elimination of isolated lakes, the LOAC-OCB model finally operates with a total of 185,945 lakes and 6,156 reservoirs.

Floodplain locations and surface areas are derived from the GLWD v2.0 dataset (Lehner et al., 2025), selecting classes corresponding to regularly or seasonally flooded riverine and palustrine systems, both forested and non-forested. This product provides the floodplains location and the surface area they cover, but does not distinguish individual units. To delineate floodplain units, we assigned a unique identifier to all floodplain nodes within the same basin, using basin HydroBASINS level 5 (Lehner and Grill, 2013) (upper panels in Fig. 4).

Runoff, the climatic driver for discharge in the model, is obtained as monthly mean (kg m^{-2} s^{-1}) from the ISIMIP3a data repository, using the WaterGAP simulations for the period 1901–2015 (Gosling et al., 2025). Annual means are calculated for each year, followed by the multi-year average. Runoff (in mm y^{-1}) is multiplied by the contributing area of each node and converted to m^3 s^{-1} to obtain discharge in the node. The total discharge considers both local discharge and contributions from the *parent* nodes upstream. Maximum discharge is estimated using the 90th percentile of monthly runoff, calculated from Fekete et al. (2002), using the Climate Data Operator (CDO) software.

Coastal nodes correspond to the terminal nodes of the river network (i.e., river mouths). Their identification required a preliminary model run to generate the network structure. Coastal units are defined by grouping terminal nodes by HydroBASINS level 5 (lower panels in Fig. 4), following the approach used for floodplains. The surface area of each coastal unit is determined by mapping the blue-carbon habitats—mangroves, saltmarshes, and seagrasses—using the World Atlas of Mangroves (Spalding et al., 2010), the Global Distribution of Saltmarshes (Mcowen et al., 2017), and the Global Distribution of Seagrasses (Short, 2020), by the World Conservation Monitoring Centre (WCMC). Habitat areas are assigned to the nearest coastal unit.

Historical monthly mean river temperatures (1901 – 2021) are derived from ISIMIP3a WaterGAP simulations (Gosling et al., 2019), while historical daily mean bottom lake temperature (1901 - 2021) are obtained from ISIMIP3a GOTM simulations (Gosling et al., 2019). Bottom temperature was considered more appropriate than surface temperature, as the focus is on mineralization processes occurring in and above deposited sediments. Annual means are calculated for each year, followed by the multi-year average.

https://doi.org/10.5194/egusphere-2025-5359
Preprint. Discussion started: 5 February 2026

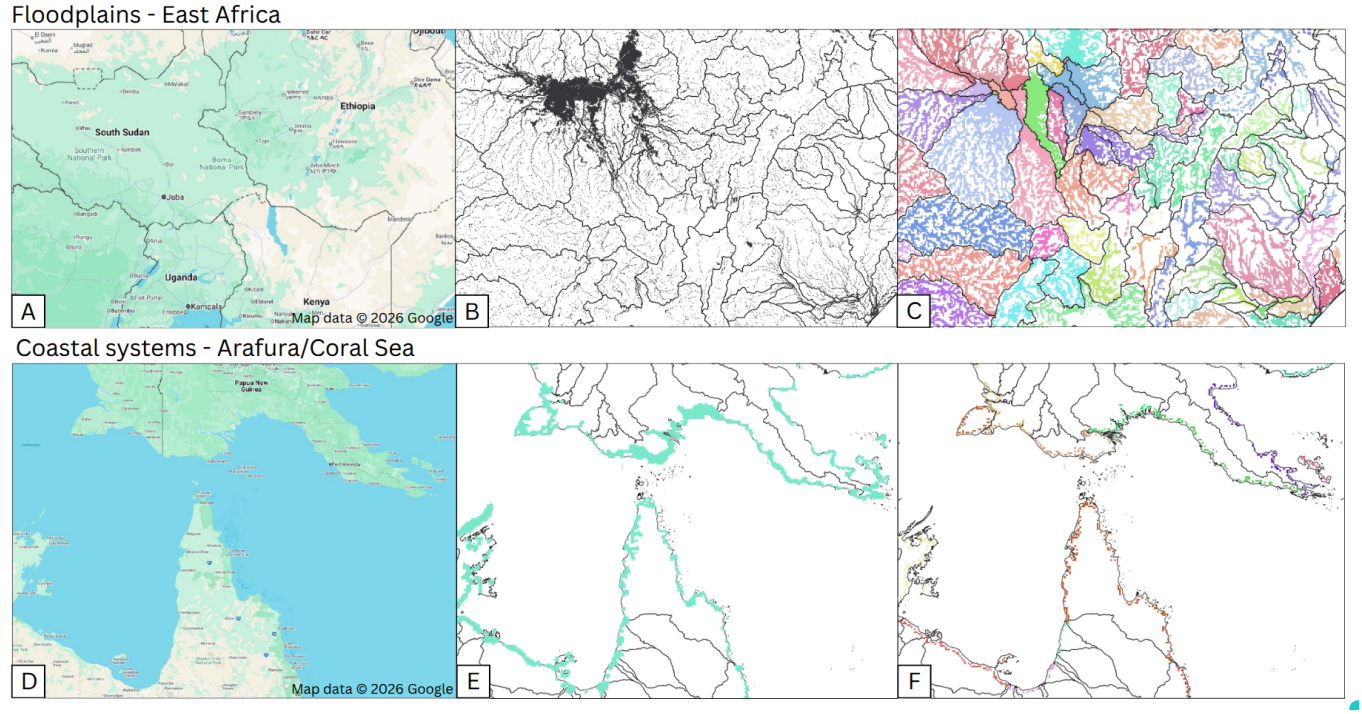

Figure 4. Examples of nodes grouped by HydroBASINS level 5 (Lehner and Grill, 2013) for floodplain and coastal system delineation. The upper panels illustrate a region in East Africa: (A) map of the area (map data © 2026 Google), (B) in black dots, floodplains from GLWD v2.0 (Lehner et al., 2025) with HydroBASINS level 5 boundaries delineated in the background, and (C) their representation in the model, where each color indicates a distinct floodplain unit. In the model, all the nodes within a floodplain unit (*dummy* and *burial*), will be classified as floodplain nodes, but only one of them will be a *burial* node, with an ecosystem area corresponding to the sum of all nodes within the floodplain unit, derived from GLWD v2.0. The lower panels show an area between Papua New Guinea and Northern Australia, including parts of the Arafura and Coral Seas: (D) map of the area (map data © 2026 Google), (E) in color, coastal habitats with HydroBASINS level 5 boundaries delineated in the background, and (F) their representation in the model, where each color indicates a distinct coastal unit.

2.5.3 Inputs step 3

Sediment loads, OC content, and particle size fractions are added at this final stage. Local sediment input at each node is estimated as the amount of soil displaced by water, expressed in Mg ha^{-1} y^{-1}, based on the RUSLE-based Global Soil Erosion Modeling platform (GloSEM, Borrelli et al. (2017)). The OC content associated with these sediment loads corresponds to the Topsoil OC product from the Harmonized World Soil Database (HWSD, Wieder et al. (2014)). The relative proportions of clay, silt and sand within the sediment loads are derived from Poggio et al. (2021). A separate sediment and OC mass balance are performed for each particle fraction, considering that their distinct settling velocities affect the calculation of sedimentation and burial at the *burial* nodes.

https://doi.org/10.5194/egusphere-2025-5359
Preprint. Discussion started: 5 February 2026

Table 1. Model raster input data

Data	Unit	Description	Source
Flow directions	-	Flow direction following the D8 method (O'Callaghan and Mark, 1984). Adapted from Dominant River Tracing (DRT, Wu et al. (2012)) to 0.0625º x 0.0625º spatial resolution.	Font et al. (2019)
Slopes	m/m	Terrain slope. Raster produced from digital elevation models from HydroSHEDS (Lehner et al., 2008) and Hydro1k (VERDIN, 2011), with a 0.0625º x 0.0625º spatial resolution.	Font et al. (2019)
Runoff	mm y^{-1}	Annual runoff from ISIMIP3a global water simulation using WaterGAP2-2e impact model driven by 20CRv3-ERA5 climate forcing, with a spatial resolution of 0.5º x 0.5º. Transformed from kg m^{-2} s^{-1}.	Gosling et al. (2025)
Runoff max	mm mo^{-1}	90th percentile of monthly runoff calculated using the Climate Data Operator (CDO) software.	This study
Ecosystem type	-	0: river, 1: lake, 2: reservoir, 3: floodplain, 4: coastal.	This study
Lake/Reservoir ID	-	Lake/Reservoir unique identification number from HydroLAKES.	Messager et al. (2016)
Lake/Reservoir volume	mcm = 0.001 km^3	Total lake or reservoir volume from HydroLAKES.	Messager et al. (2016)
Lake/Reservoir depth	m	Average lake or reservoir depth from HydroLAKES.	Messager et al. (2016)
Lake/Reservoir area	km^2	Average lake or reservoir area from HydroLAKES.	Messager et al. (2016)
Lake/Reservoir catchment area	km^2	Area of the total upstream catchment(s) from HydroLAKES.	Messager et al. (2016)
Floodplain area	ha x 10	Absolute area of all wetland classes combined from the Global Lakes and Wetlands Dataset (GLWD v2.0) with a 15 arc-seconds (∼ 500 m) spatial resolution.	Lehner et al. (2025)

Table continued on next page

https://doi.org/10.5194/egusphere-2025-5359
Preprint. Discussion started: 5 February 2026

Model raster input data (continued)

Data	Unit	Description	Source
Floodplain ID	-	Floodplain unique identification number. Classes 10, 11, 12, 13, 16 and 17 from GLWD v2.0 (Lehner and Döll, 2004) with a 15 arc-seconds (∼ 500 m) spatial resolution are considered to identify floodplains location. They are delimited to basins level 5 from HydroBASINS (Lehner and Grill, 2013) to get individual units.	This study
Coastal ID	-	Coastal unique identification number. Nodes discharging to the ocean are delimited to basins level 5 from HydroBASINS to get individual units.	This study
Coastal area	km^2	Mangrove, saltmarsh, and seagrass areas associated to the same coastal ID. Original data from the World Atlas of Mangroves (Spalding et al., 2010), the Global Distribution of Saltmarshes (Mcowen et al., 2017) , and the Global Distribution of Seagrasses Short (2020), respectively. Input as csv format.	This study
Coastal type	-	Defined by the coastal habitats associated to the same coastal ID	This study
Sediment input	Mg ha^{-1} y^{-1}	Locally generated sediment from (soil) erosion displaced by water, estimated through the RUSLE-based modeling approach, with a 25 x 25 km (∼ 0.2083º) spatial resolution.	Borrelli et al. (2017)
OC content input	% weight	Topsoil organic carbon from the Harmonized World Soil Database (HWSD) v1.2, based on the carbon content of the dominant soil type.	Wieder et al. (2014)
Clay/Silt/Sand content input	g kg^{-1}	Proportion of clay/silt/sand particles in the fine earth fraction from SoilGrids 2.0 with a 1 x 1 km spatial resolution (aggregated from a 250 x 250 m resolution). This is assumed to be the same for the locally generated sediments.	Poggio et al. (2021)

Table continued on next page

https://doi.org/10.5194/egusphere-2025-5359
Preprint. Discussion started: 5 February 2026

Model raster input data (continued)

Data	Unit	Description	Source
Bottom lake temperature	K	Yearly mean bottom temperature derived from ISIMIP3a daily global lake simulation using GOTM impact model driven by 20CRv3-ERA5 climate forcing, with a spatial resolution of 0.5º x 0.5º.	Golub et al. (2022)
River temperature	K	Yearly mean river temperature derived from ISIMIP3a monthly global river simulation using WaterGAP2-2e impact model driven by 20CRv3-ERA5 climate forcing, with a spatial resolution of 0.5º x 0.5º.	Gosling et al. (2025)

3 Model validation

To validate the performance of the LOAC-OCB model, we conducted a multi-faceted validation using independent global datasets and previously published studies. First, we compared modeled river discharge and sediment export at the mouths of the largest rivers with values reported in global observational studies. Second, we assessed the distributions of LSR and OCB against a previously compiled global observation dataset (Henry et al., 2024).

3.1 Discharge, sediment loads and sediment concentrations

For this validation, we used the study by Dethier et al. (2022), which uses satellite-based estimates of suspended sediment concentration and flux for over 400 major river mouths worldwide. We also compared the discharge values used in their analysis, derived from the dataset by Fekete et al. (2002). For each observation point, we computed the annual mean for each year and then calculated the overall multi-years average. From 371 discharge points, 94% percent of the modeled values were within one order of magnitude of the observed estimates (Fig. 5(A)). From 276 sediment load and sediment concentration points, 64% and 72% of the modeled values were within one order of magnitude of the observed estimates, respectively (Fig. 5 (B and C)). Sediment concentration was compared to provide a reference relative to water volume, helping distinguish whether differences in sediment loads are driven by discrepancies in discharge or sediment content per unit water. At sites with the largest deviations between observed and modeled values, the model tends to overestimate runoff in the lower quantiles and underestimate it in the higher quantiles. In regions with low runoff and flat topography, runoff estimates and river network routing are less reliable, and these errors propagate to sediment loads and concentrations (Fig. 5).

https://doi.org/10.5194/egusphere-2025-5359
Preprint. Discussion started: 5 February 2026

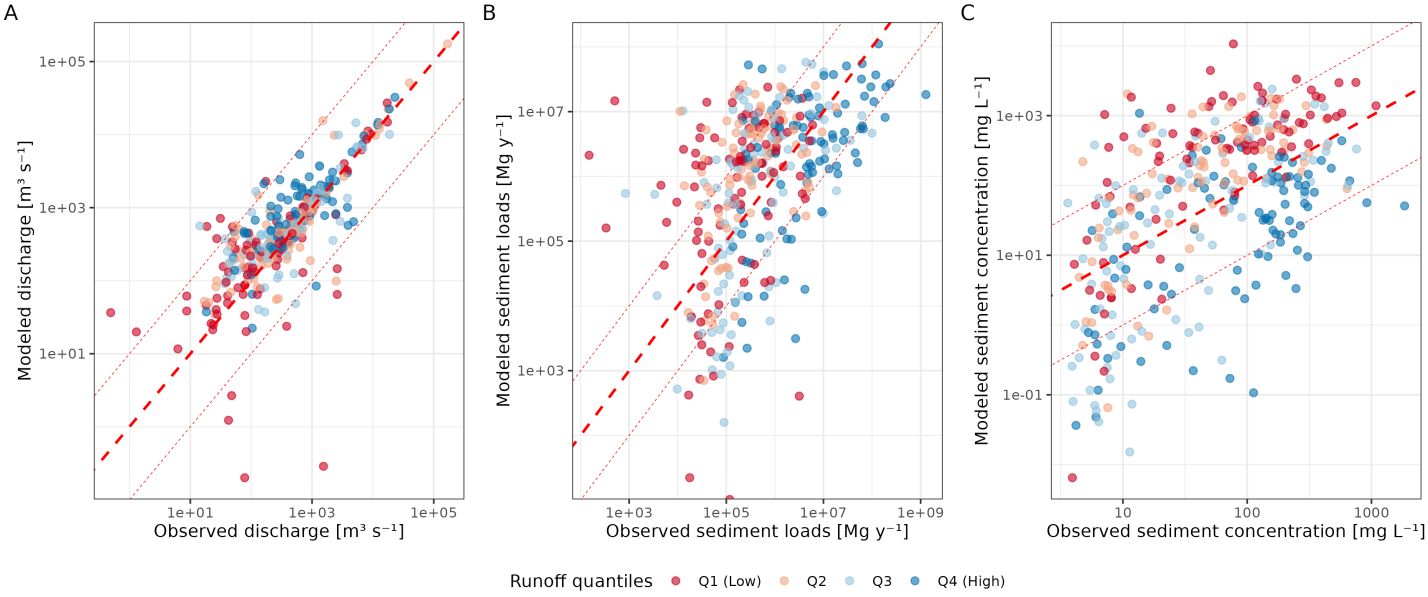

Figure 5. Modeled versus observed values for (A) annual mean discharge, (B) sediment load, and (C) sediment concentration. Each point represents a river mouth. Observed data are from Dethier et al. (2022). The bold red dashed line represents the 1:1 line, while the light red dotted lines indicate a deviation of one order of magnitude. Points are colored by runoff quantiles, with red representing the lowest and blue the highest.

3.2 LSR and OBC rates

The LOAC-OCB model is not intended to provide precise burial rates for individual systems, but rather to quantify the relative distribution of terrestrial OC along the LOAC depositional environments. To exemplify the use of LOAC-OCB, a total of over 2.4 million nodes were processed, including 170,997 lakes, 6,000 reservoirs, 4,033 floodplains, and 377 coastal ecosystems, and the underlying river network connecting them. To evaluate model performance, we compared values and distributions of LSR and OCB generated by LOAC-OCB with those from the global observational dataset (Fig. 6) compiled in a previous work (Henry et al., 2024).

Modeled LSR varies within one order of magnitude across ecosystem types (Fig. 6). The highest median rates were found in reservoirs (9.22 ± 0.04 mm y^{-1}, standard error of the median estimated by bootstrap) and coastal systems (5.13 ± 0.80 mm y^{-1}), while the lowest rates occurred in lakes (0.307 ± 0.003 mm y^{-1}) and floodplains (0.49 ± 0.03 mm y^{-1}). Observed values follow a similar pattern: highest medians in reservoirs (10.80 ± 2.95 mm y^{-1}) and coastal systems (4.55 ± 0.55 mm y^{-1}), and lowest in lakes (2.00 ± 0.60 mm y^{-1}) and floodplains (3.75 ± 0.42 mm y^{-1}).

Modeled OC_{bur} follow the same trend. Reservoirs showed the highest median OC_{bur} (94.30 ± 3.85 g C m^{-2} y^{-1}), followed by coastal systems (53.1 ± 14.7 g C m^{-2} y^{-1}), floodplains (1.75 ± 0.11 g C m^{-2} y^{-1}) and lakes (1.19 ± 0.02 g C m^{-2} y^{-1}) (filled

https://doi.org/10.5194/egusphere-2025-5359
Preprint. Discussion started: 5 February 2026

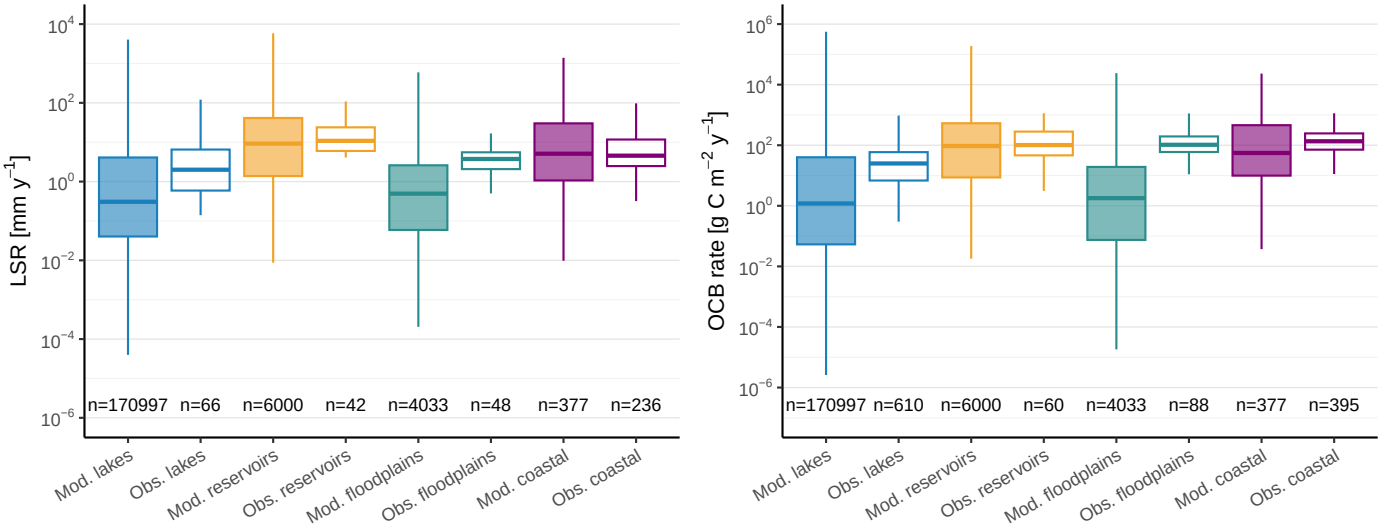

Figure 6. Modeled and observed Linear Sedimentation Rate (LSR) and Organic Carbon Burial (OCB) rate by ecosystem type in different colors. Filled and empty boxes are modeled and observed values, respectively. n is the number of modeled systems.

boxes in Fig. 6). Observed values are about one order of magnitude higher, with highest medians in coastal systems (134.0 ± 10.3 g C m^{-2} y^{-1}), followed by floodplains (104.0 ± 12.7 g C m^{-2} y^{-1}), reservoirs (101.0 ± 28.3 g C m^{-2} y^{-1}), and lakes (25.0 ± 1.4 g C m^{-2} y^{-1}).

The observed distributions of LSR and OCB for reservoirs and coastal ecosystems fully overlap with the modeled distributions, showing strong agreement. For lakes, observed distributions also overlap with modeled distributions but primarily at the upper end of values. We attribute this to several factors. First, LOAC-OCB excludes lakes smaller than 0.1 km^2 due to the HydroLAKES minimum size threshold. The fact that small lakes can exhibit high LSR (Fig. A1), implies that excluding them might be a reason for lower modeled than observed median LSR and OCB. Second, the enormous amount of lakes involves large heterogeneity in OC dynamics that might not be fully captured by the limited number of observational studies we used to fit our burial functions. In practice, OCB studies tend to target systems known or presumed to have significant OC loads, introducing a bias in the observed dataset toward smaller systems with higher OC content (Fig. A2), and therefore, higher OCB (Fig. A3 and A4). Third, most of reported LSR and OCB values in the literature include OC buried from both allochthonous (e.g., POC from soils) and autochthonous (e.g., phytoplankton production) OC sources, whereas LOAC-OCB considers allochthonous (i.e., terrestrial) OC only. This might have a stronger effect in lakes with longer residence times where autochthonous OC can become more relevant (Hanson et al., 2014), in contrast to reservoirs, which in general have shorter residence times and are mostly governed by allochthonous OC (Maavara et al., 2017) (Fig. A5).

Floodplains exhibit the largest discrepancies between modeled and observed rates. Modeled distributions of LSR and OCB are lower, with mean values approximately one order of magnitude below those in the observational dataset. This mismatch

https://doi.org/10.5194/egusphere-2025-5359
Preprint. Discussion started: 5 February 2026

likely reflects the scarcity of empirical data on floodplain sedimentation and OC dynamics, with far fewer LSR and OCB measurements than in other ecosystems, which makes global representation uncertain (Henry et al., 2024). Additionally, unlike lakes and reservoirs, floodplains lack well-defined spatial boundaries. In LOAC-OCB, these systems are represented using relatively large units (with a median of 3306 km^2), whereas most field studies focus on smaller areas. For instance, a study in the Congaree River used representative areas of 2.4 - 44 km^2 (Ricker and Lockaby, 2015); while a study in the Danube River covered 13.2 km^2. In contrast, huge river-floodplain systems such as the Okavango Delta, Rhine, and Amazon extend across $\sim$ 15,000 km^2 (Bernal and Mitsch, 2013), 125,000 km^2 (Hoffmann et al., 2013), and 6,000,000 km^2 (Sanders et al., 2017), respectively. These large discrepancies in spatial scale between modeled units and field observations likely influence their comparability. This should not be interpreted as a shortcoming of either approach but as a consequence of their intrinsic differences in scale and methodology.

Another source of uncertainty, which affects mostly to lakes and floodplains, relates to the simplified river network topology required for the global modeling. Although isolated systems and those likely spatially misaligned were already excluded, this does not guarantee that some of the depositional ecosystems assigned to a particular node are actually located directly along the main river channel. LOAC-OCB assumes that all water and sediments entering a node pass through the main stem of the river network, which may not always reflect reality. In most occasions, those misalignments mean a large discharge entering an ecosystem that in reality has a much lower water input, which would imply a residence time much shorter than the actual one. This can result in underestimated burial, particularly when residence times are insufficient for significant sedimentation to occur.

Reservoirs, in contrast, are generally better represented in the model, as they are typically constructed on main river channels. The equations used for sediment retention in both lakes and reservoirs are derived from reservoir-based studies (Gill, 1979), which may also contribute to more realistic estimates in reservoirs than in natural lakes. Similarly, coastal systems are also relatively well represented due to their large spatial scales and the fact that they receive riverine exports directly at the river mouths, conditions well suited to the model's resolution and design.

3.3 OCBE

The OCBE represents the proportion of OC that is buried relative to the total OC reaching the sediment-water interface (Henry et al., 2024). This metric provides a valuable basis for comparing the relative burial capacity of different aquatic systems, especially when absolute OCB rates are not directly comparable due to substantial differences in ecosystem size, type or OC inputs. Modeled OCBE values showed a wide range across ecosystem types: 3.4 - 48.0% in lakes, 30.0 - 82.5% in reservoirs, 4.4 - 40.0% in floodplains, and 43.1 - 89.0% in coastal ecosystems, these ranges representing the 25th to 75th percentiles of each distribution (Fig. 7). Among all ecosystem types, coastal ecosystems and reservoirs showed the highest burial efficiencies, burying on average 59.6% and 55.4% of the OC that reaches the sediment, respectively, whereas floodplains (26.3%) and lakes (27.5%) exhibited substantially lower efficiencies.

https://doi.org/10.5194/egusphere-2025-5359
Preprint. Discussion started: 5 February 2026

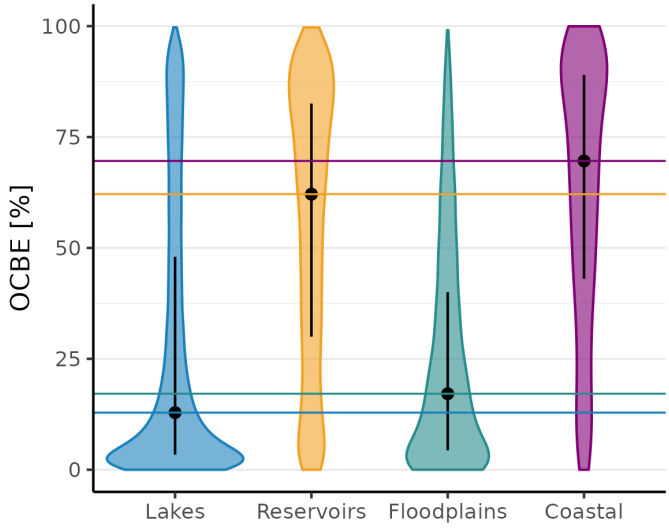

Figure 7. Organic Carbon Burial Efficiency (OCBE) by ecosystem type. Violin plots show the distribution of modeled OCBE (%) for each ecosystem type. The width of each violin represents the density of observations at a given value. Black vertical lines within each violin indicate the inter-quartile range (25th – 75th percentiles), with a central point marking the median value for that ecosystem.

3.4 OC mineralization

In LOAC-OCB, total mineralization of terrestrial POC includes processes occurring both in the water and within the sediments. Among ecosystem types, reservoirs exhibited the highest median OC mineralization rate at 160.0 ± 2.8 mg C m^{-2} d^{-1}, followed by coastal ecosystems (80.1 ± 6.8 mg C m^{-2} d^{-1}), floodplains (24.1 ± 1.0 mg C m^{-2} d^{-1}), and lakes (22.9 ± 0.2 mg C m^{-2} d^{-1}) (Fig. 8). These values consistent with reported ranges in the literature. For instance, individual lakes worldwideshow CO_2 and CH_4 emissions ranging from 13.7 mg C m^{-2} d^{-1} in Lake Baikal to 435.6 mg C m^{-2} d^{-1} in lake Kinneret (Sobek et al., 2009, 2011; Ferland et al., 2014), while the Mascarenhas de Moraes reservoir reports mean CO_2 and CH_4 emissions of 94.3 mg C m^{-2} d^{-1} (Mendonça et al., 2016). Regarding coastal ecosystems, Siikamäki et al. (2013) estimated total CO_2 emissions of 0.076 Pg C y^{-1} for mangroves, saltmarshes and seagrasses. When averaged over their reported area (509,170 km^2), this corresponds to an approximate mean emission rate of 408.9 mg C m^{-2} d^{-1} — about five times higher than our estimates. This discrepancy is likely due to the significant contribution of autochthonous OC emissions in coastal ecosystems, which are not accounted for in LOAC-OCB. In addition, future developments could explore adapting mineralization formulations to better reflect the specific conditions and dominant processes of each depositional environment.

3.5 Global OC fluxes

When scaled to their total modeled surface areas, estimated global OCB fluxes were 0.97 Pg C y^{-1} for floodplains (8,363,169 km^2), 0.72 Pg C y^{-1} for reservoirs (253,404 km^2), 0.51 Pg C y^{-1} for lakes (2,061,552 km^2), and 0.30 Pg C y^{-1} in coastal

https://doi.org/10.5194/egusphere-2025-5359
Preprint. Discussion started: 5 February 2026

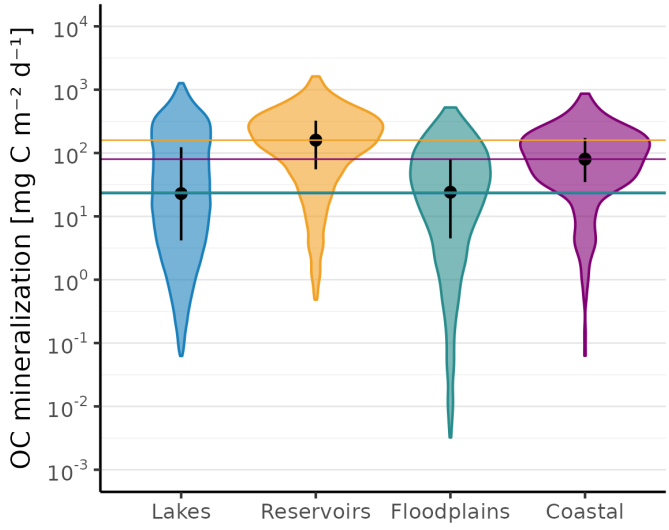

Figure 8. OC mineralization by ecosystem type. Violin plots show the distribution of modeled OC mineralization rated (mg C m^{-2} d^{-1}) for each ecosystem type. Values outside the 1–99 percentile range were excluded to remove extreme outliers and improve visualization of the main distribution. The width of each violin represents the density of observations at a given value. Black vertical lines within each violin indicate the inter-quartile range (25th – 75th percentiles), with a central point marking the median value for that ecosystem.

ecosystems (873,923 km^2). This yields a LOAC contribution of 2.51 Pg C y^{-1} to the global OCB budget, highlighting the major role of floodplains, driven largely by their extensive spatial coverage despite relatively low areal OCB rates. Reservoirs, in contrast, represent a much smaller surface area and contribute disproportionately to global OCB due to their high sediment trapping efficiency and LSR. Overall, we estimated that the LOAC receives 345.54 Pg y^{-1} of sediment from the terrestrial systems through erosion, with the OC fraction corresponding to 4.82 Pg C y^{-1} (1.39%). Of this terrestrial POC load, 2.51 Pg C y^{-1} is buried within the sediments, 1.54 Pg C y^{-1} is mineralized, and 0.79 Pg C y^{-1} is exported to the open ocean. These values are consistent with previous global assessments: Drake et al. (2018) estimated that soils export 5.1 Pg C y^{-1} to rivers, while Liu et al. (2024) reported that 1.02 Pg C y^{-1} reaches the ocean, though both included inorganic as well as organic fractions (Table 2).

Many studies have reported global OCB estimates (Table 2), although they do not include all the ecosystem types present in LOAC-OCB. For instance, Regnier et al. (2022) estimated that inland waters, estuaries and tidal wetlands bury 0.25 ± 0.15 Pg C y^{-1}. While this value is lower than ours, it excludes floodplains and is not directly comparable, as their approach considered additional forms of C (i.e., dissolved inorganic carbon (DIC), DOC and POC), estimated lower terrestrial OC input (4.1 ± 1.5 Pg C y^{-1}), and a higher OC mineralization rate (1.85 ± 0.5 Pg C y^{-1}).

For coastal systems, OCB estimates vary widely. Lovelock and Reef (2020) reported 0.03 - 0.07 Pg C y^{-1}, Duarte et al. (2013) estimated 0.08 - 0.22 Pg C y^{-1}, and Twilley et al. (1992) suggested 0.41 Pg C y^{-1}. Our estimate is in the upper end of these ranges with 0.30 Pg C y^{-1}. These studies generally do not distinguish the source of OC, and the relative contribution of

https://doi.org/10.5194/egusphere-2025-5359
Preprint. Discussion started: 5 February 2026

Table 2. Global organic carbon (OC) fluxes (Pg C y^{-1}) across LOAC ecosystems and comparison with previous studies.

OC flux	LOAC-OCB	Other studies	Reference
OC input to LOAC	4.82	4.1 - 5.1	Drake et al. (2018); Regnier et al. (2022)
OCB floodplains	0.97	0.5 - 1.5	Aufdenkampe et al. (2011)
OCB reservoirs	0.72	0.35	Li 2022
OCB lakes + reservoirs	1.23	0.06 - 0.6	Mendonça et al. (2017); Tranvik et al. (2009)
OCB coastal ecosystems	0.30	0.03 - 0.41	Duarte et al. (2013); Lovelock and Reef (2020); Twilley et al. (1992)
OCB LOAC	2.51	0.25 ± 0.15	Regnier et al. (2022)
OC mineralization	1.57	1.4 - 3.9	Drake et al. (2018); Lal (2003); Regnier et al. (2022); Tranvik et al. (2009)
OC export to ocean	0.79	1.02	Liu et al. (2024)

autochthonous biomass remains poorly constrained (Li et al., 2022). Since autochthonous OC is more labile, it is more prone to degradation compared to terrestrial POC transported over long distances.

For reservoirs, Li et al. (2022) estimated using a process-based model that 0.35 Pg POC y^{-1} is trapped in reservoirs, which is approximately half of our estimate (0.72 Pg C y^{-1}). Their study is methodologically comparable to ours; however, their estimated sediment input (22.8 Pg y^{-1}) is substantially lower than ours (345.54 Pg y^{-1}), likely because they did not include sediments generated from floodplain erosion, which could explain the large discrepancy between the two estimates. Mendonça et al. (2017) and Tranvik et al. (2009) also reported lower OCB rates for lakes and reservoirs combined, ranging from 0.06 - 0.25 Pg C y^{-1} and 0.6 Pg C y^{-1}, respectively. Nevertheless, these were studies based on extrapolation from observational datasets and on a mass-balance approach, respectively .

Finally, regarding floodplains, Aufdenkampe et al. (2011) suggested that 0.5 - 1.5 Pg C y^{-1} are buried in hillslopes and floodplains, while we estimate a mean OCB flux of 0.97 g C y^{-1} in riverine floodplains. To date, floodplains have not been explicitly included in long-term OCB modeling frameworks (Hoffmann et al., 2013). Our results indicate that LOAC-OCB provides a promising approach to incorporate floodplains, as the modeled values are broadly consistent with previous large-scale estimates.

Global OC mineralization fluxes were estimated at 1.57 Pg C y^{-1}, partitioned as follows: 1.11 Pg C y^{-1} in floodplains, 0.08 Pg C in rivers, 0.19 Pg C y^{-1} in lakes, 0.11 Pg C y^{-1} in reservoirs, and 0.07 Pg C y^{-1} in coastal ecosystems. For comparison, Lal (2003) estimated that 0.8 - 1.2 Pg C y^{-1} of terrestrial OC is emitted to the atmosphere due to lateral transport induced by erosion, a range slightly lower than our estimate. However, this study does not account for within-system mineralization and includes both dissolved and particulate forms of terrestrial OC. In contrast, Tranvik et al. (2009) estimated 1.4 Pg C y^{-1} of

https://doi.org/10.5194/egusphere-2025-5359
Preprint. Discussion started: 5 February 2026

allochthonous C is emitted from inland waters (lakes and streams), while Drake et al. (2018) reported a substantially higher outgassing flux of 3.9 Pg C y^{-1}, suggesting that even these estimates may be conservative. These latter two studies, however, are conceptual and do not distinguish among C forms. This likely explains why our results are lower: on the one hand, the LOAC-OCB does not account for C emission from inorganic processes, which can be substantial at a global scale (Marcé et al., 2015), and on the other hand, the model only includes mineralization of terrestrial OC, when the autochthonous fraction is the most labile portion and therefore most prone to mineralization, especially in natural lakes where autochthonous OC input plays a more relevant role (Figure A5).

4 Conclusions and further development

This study presents LOAC-OCB, the first global model to quantify particulate terrestrial OCB across the diverse ecosystems of the LOAC—lakes, reservoirs, floodplains, and coastal ecosystems—within a unified framework. Our results reveal substantial differences in OCB rates and OCBE among aquatic ecosystems, shaped by hydrological (i.e., runoff), morphological (i.e., water depth, ecosystem area), sedimentary (i.e., erosion, particle size, OC content) and spatial (i.e., water temperature) factors. The model can capture how sedimentation and burial processes occurring in one part of the LOAC influence fluxes and pools downstream, making it a powerful tool for understanding interactions among interconnected ecosystems when assessing global OCB. Differences between our results and previous estimates are expected, as earlier studies typically focused on isolated systems, whereas LOAC-OCB explicitly captures interactions and cumulative effects across interconnected ecosystems.

LOAC-OCB offers a versatile framework for future research and development. Beyond global quantification and spatial distribution of LSR, OCB, and OCBE, the model allows various applications. One of them is to evaluate the anthropogenic impact on OCB redistribution, for example, the global proliferation of man-made reservoirs, which has fundamentally altered sediment and associated C dynamics. While it is well established that reservoirs retain sediments and promote OC burial, the counterfactual remains unresolved: in the absence of reservoirs, what would have happened to this OC? Would it have been mineralized and emitted to the atmosphere, or buried elsewhere within the LOAC? Addressing such questions is essential to constrain the net role of human activities in global C cycling.

In addition, LOAC-OCB could be extended to long-term simulations or applied to climate and land-use change scenarios. For these applications, a thorough uncertainty quantification would be necessary, to account for the propagation of input and parameter uncertainties through the model and ensure robust predictions. In this context, certain state variables could be treated as non-steady, for example, reservoir water volume could vary over time, altering residence time and, consequently, C sedimentation and burial. Such extensions would help to assess the resilience or vulnerability of OC sinks under future conditions. As more empirical data on OCBE become available, especially in freshwater systems, the model can be refined and further validated to improve accuracy and applicability. Its modular structure allows classification of ecosystems into archetypes (e.g., coastal types or floodplain morphologies), supporting the derivation of type-specific OCB estimates. This can strengthen environmental assessments in data-scarce regions and inform global decision-making.

https://doi.org/10.5194/egusphere-2025-5359
Preprint. Discussion started: 5 February 2026

Some aspects of LOAC-OCB can still be improved. The current parametrization of sedimentation is based only on data from lakes and reservoirs. Expanding empirical datasets for OCBE in floodplains and coastal systems would strengthen the robustness of the model's assumptions and increase the reliability of its results. In addition, promoting OCBE as a common metric could improve comparability across ecosystem types and enhance global OCB assessments. If OCBE were routinely measured in freshwater and coastal environments, it would facilitate extrapolation to data-poor regions and improve the consistency of global C budget estimates.

Ultimately, LOAC-OCB provides a foundation for a more integrated understanding of aquatic C cycling and its role in global climate dynamics, bridging key knowledge gaps and advancing the representation of inland and coastal processes in Earth system models.

Code and data availability. The LOAC-OCB model (version 1.0) source code, user manual, and all input and output data are available on Zenodo (EU Open Research Repository - DOI: 10.5281/zenodo.17476678, (Henry, 2025)). All materials are distributed under the Creative Commons Attribution 4.0 International License (CC BY 4.0).

https://doi.org/10.5194/egusphere-2025-5359
Preprint. Discussion started: 5 February 2026

Appendix A: Other plots

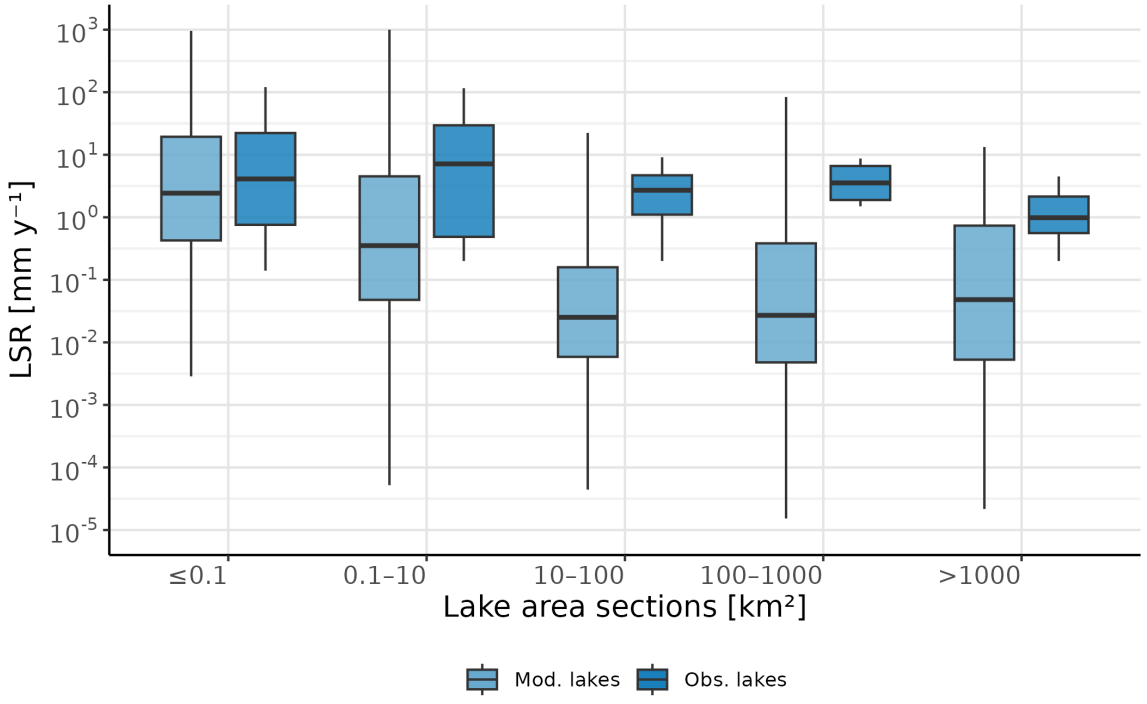

Figure A1. Boxplots of lake linear sedimentation rates (LSR) across lake size classes. Lakes are grouped into five area-based sections: ≤0.1, 0.1–10, 10–100, 100–1000, and >1000 km^2. Note that in the first section, modeled values can only correspond to lakes with a surface area equal to 0.1 km^2.

https://doi.org/10.5194/egusphere-2025-5359
Preprint. Discussion started: 5 February 2026

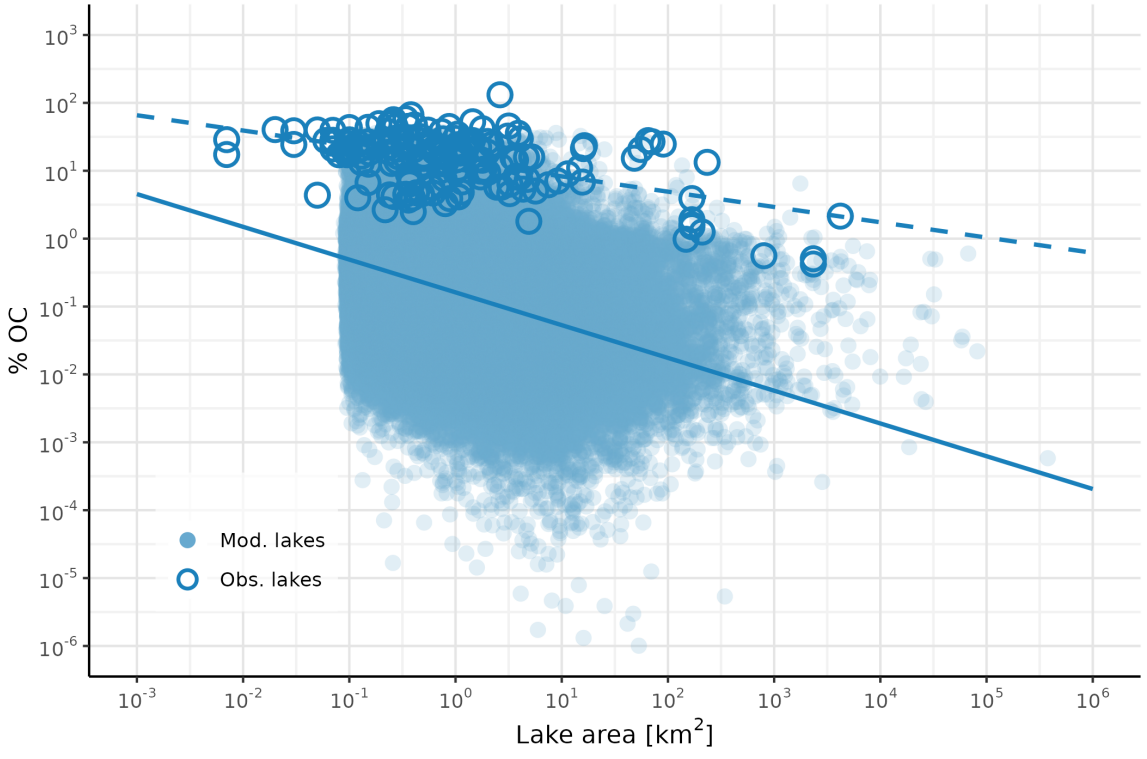

Figure A2. Scatterplot of organic carbon content (%OC) versus lake area for modeled (semi-transparent points) and observed (outlined points) lakes. Solid and dashed lines show the regression trends for modeled and observed lakes, respectively.

https://doi.org/10.5194/egusphere-2025-5359
Preprint. Discussion started: 5 February 2026

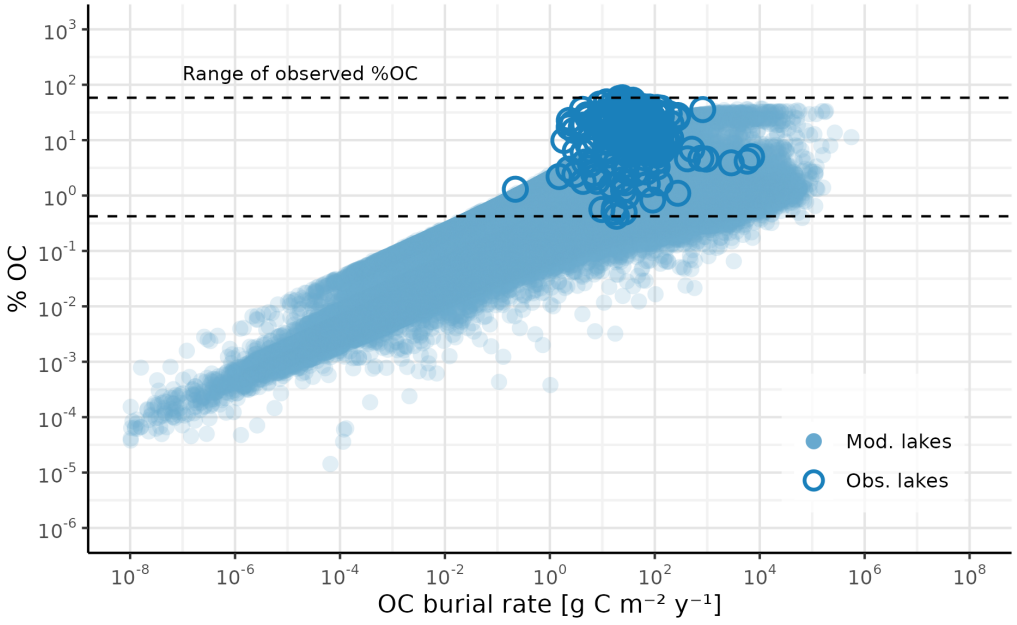

Figure A3. Scatterplot of organic carbon burial (OCB) rate versus organic carbon content (%OC) in lakes. Modeled lakes are shown as semi-transparent points, while observed lakes are shown as outlined points. The black dashed horizontal lines indicate the full range of %OC measured in observed lakes.

https://doi.org/10.5194/egusphere-2025-5359
Preprint. Discussion started: 5 February 2026

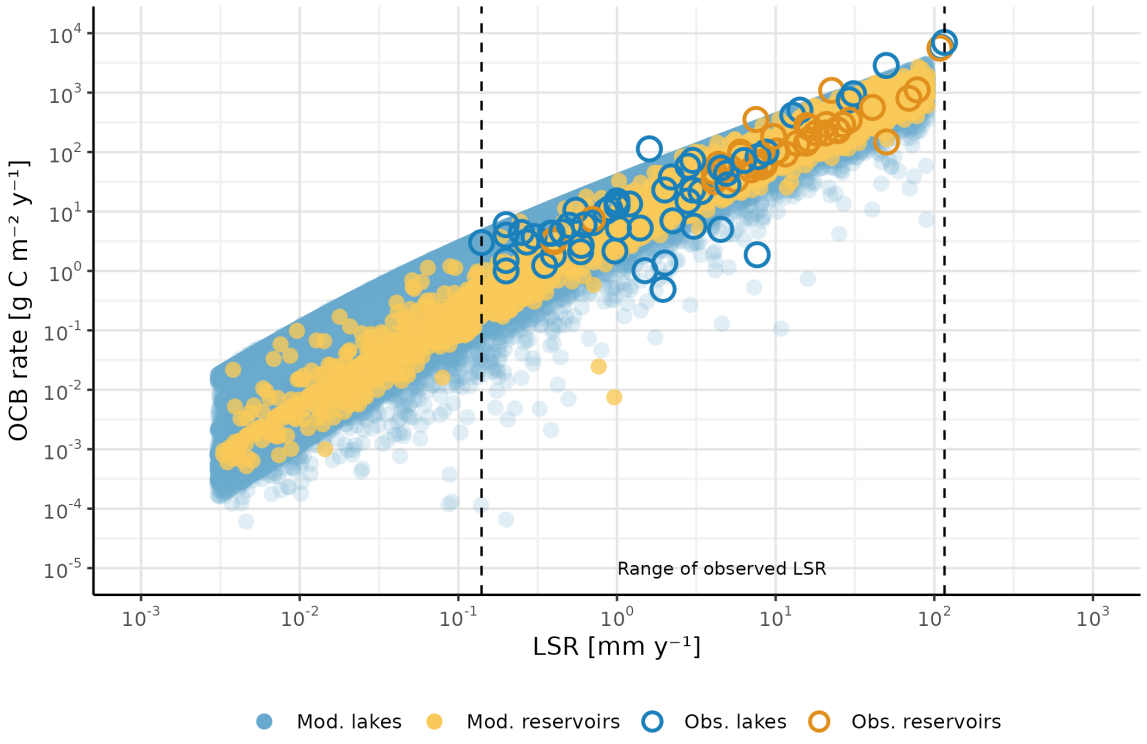

Figure A4. Relationship between linear sedimentation rate (LSR) and organic carbon burial (OCB) rate for lakes and reservoirs. Modeled data are shown as filled circles and restricted to the 5th–95th percentile range of LSR values, highlighting the central distribution of modeled conditions and minimizing the influence of extreme outliers that can obscure general trends. Observed data (open circles) are plotted in full for reference. Black dashed vertical lines indicate the observed LSR range across all lake and reservoir measurements. This percentile-based filtering focuses the analysis on the most representative range of modeled conditions while maintaining observed variability for contextual interpretation.

https://doi.org/10.5194/egusphere-2025-5359
Preprint. Discussion started: 5 February 2026

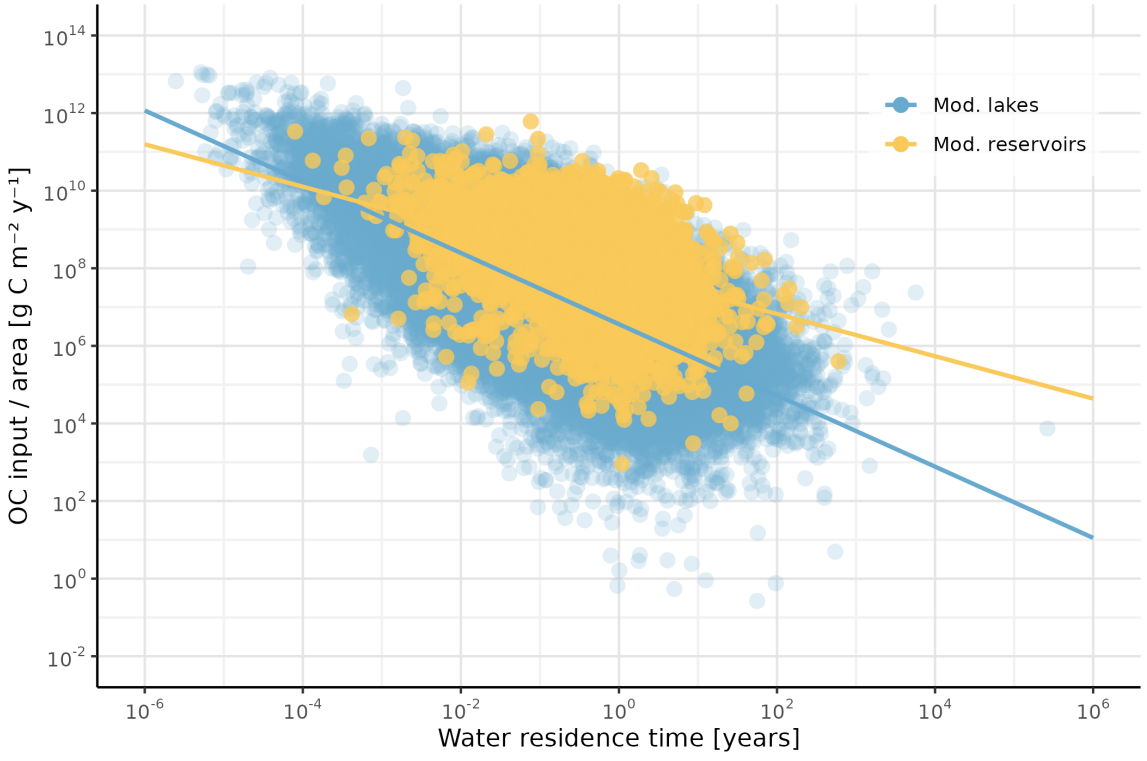

Figure A5. Relationship between water residence time (RT) and organic carbon (OC) input per unit surface area for modeled lakes and reservoirs. Each point represents a modeled system, and solid lines represent log–log linear regressions fitted separately for lakes and reservoirs. The analysis reveals how OC input rates vary with hydrological residence time, reflecting differences between lentic and impounded systems. The use of modeled data isolates the mechanistic relationship between RT and OC loading.

https://doi.org/10.5194/egusphere-2025-5359
Preprint. Discussion started: 5 February 2026

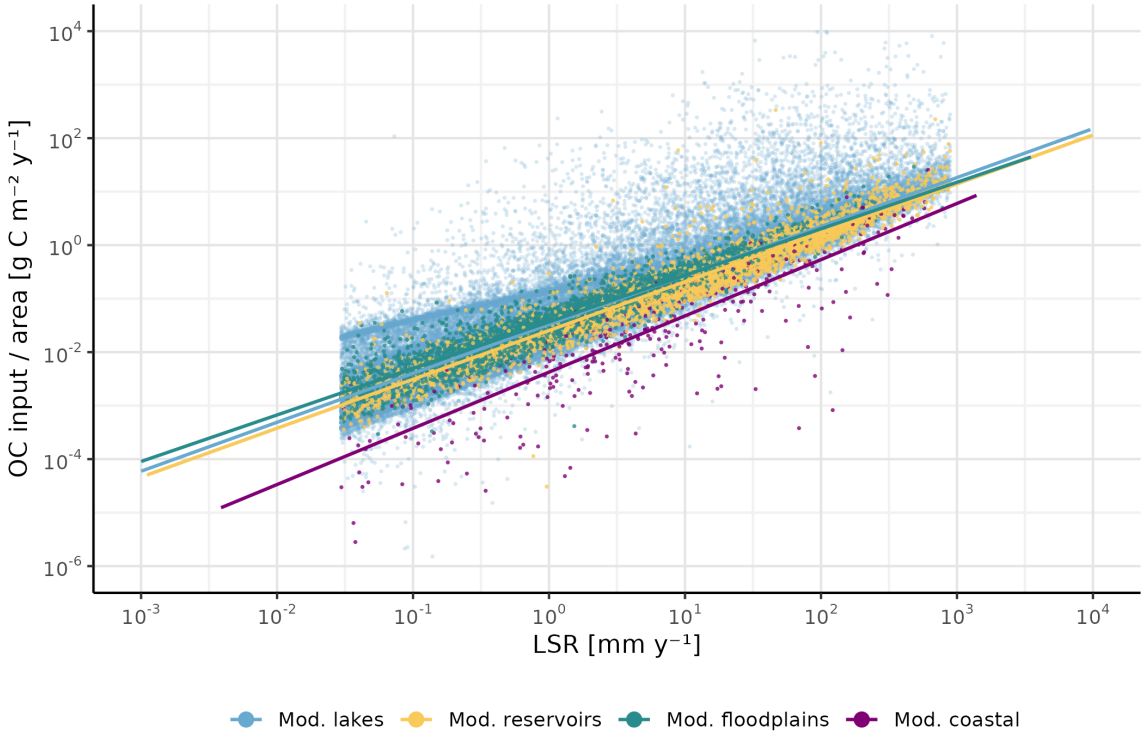

Figure A6. Scatterplot of linear sedimentation rate (LSR) versus OC input per unit area for all modeled aquatic ecosystems. Only the central 5–95% of LSR values are shown to reduce the influence of extreme values and better highlight the general relationship. Linear regression lines are added for each group to illustrate scaling trends across the full dataset.

https://doi.org/10.5194/egusphere-2025-5359
Preprint. Discussion started: 5 February 2026

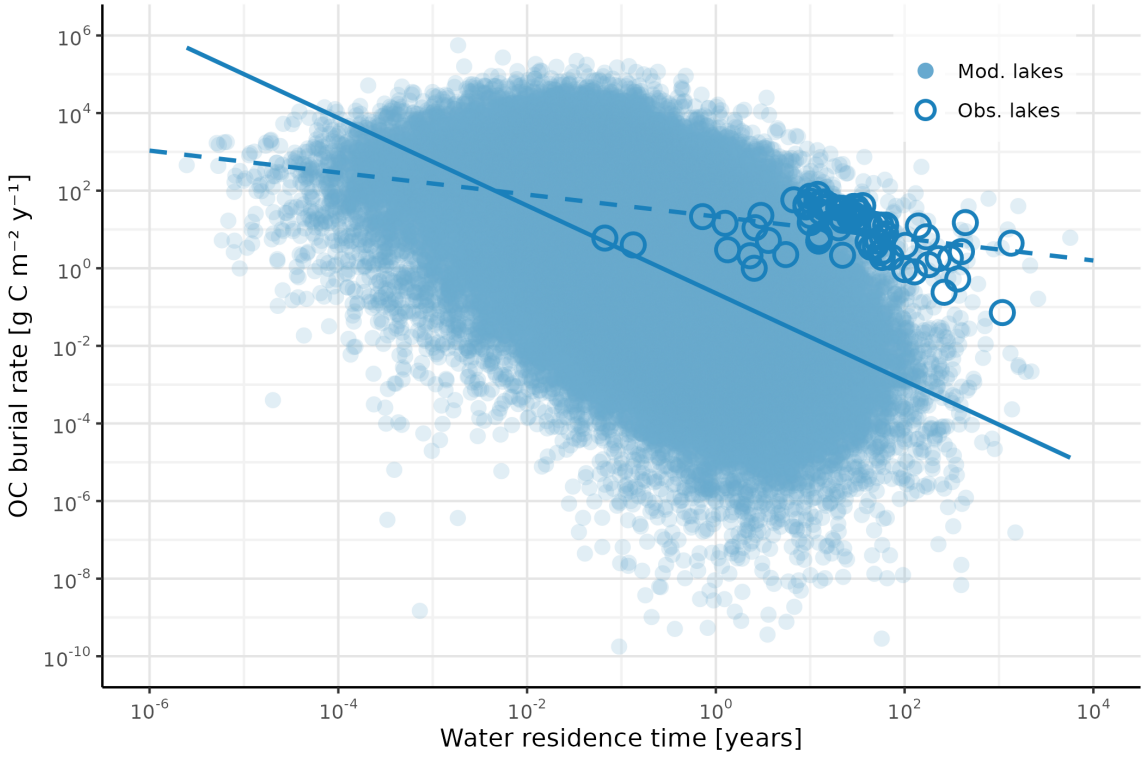

Figure A7. Relationship between water residence time (RT) and organic carbon burial (OCB) rate for lakes. Modeled systems are shown as semi-transparent filled circles in the background, while observed systems are represented by open circles. The solid line represents the log–log linear regression fitted to the modeled data, whereas the dashed line extends the regression fitted to the observed data.

https://doi.org/10.5194/egusphere-2025-5359
Preprint. Discussion started: 5 February 2026

Appendix B: Other tables

Table B1. Model variables – part 1.

Model's variable name	Unit	Description	Calculation/Equation	Reference
Ar_clay	-	Archimedes buoyancy for clay	$Ar_{\text{clay}} = \frac{\delta_{\text{clay}} - \delta_{\text{w}}}{\delta_{\text{w}}} \cdot g \cdot \frac{r_{\text{clay}}^3}{\nu^2}$	Ahrens 2003
Ar_sand	-	Archimedes buoyancy for sand	$Ar_{\text{sand}} = \frac{\delta_{\text{sand}} - \delta_{\text{w}}}{\delta_{\text{w}}} \cdot g \cdot \frac{r_{\text{sand}}^3}{\nu^2}$	Ahrens 2003
Ar_silt	-	Archimedes buoyancy for silt	$Ar_{\text{silt}} = \frac{\delta_{\text{silt}} - \delta_{\text{w}}}{\delta_{\text{w}}} \cdot g \cdot \frac{r_{\text{silt}}^3}{\nu^2}$	Ahrens 2003
area_ancestors	km^2	sum of accumulated ancestors area and node area	sum of all ancestors using function "ancestors" from networkx package and the current node area	this study
area_flood_sums	km^2	floodplain area	sum of all floodplain areas with the same floodplain ID	Lehner et al. (2025)
area_node	km^2	node area	given for the graph using function "cell_dimensions"	this study
area_system	m^2	system area for lakes and reservoirs	$A_{\text{system}} = V_{\text{system}}/D_{\text{w}}$	this study
	m^2	system area for floodplains	$A_{\text{system}} = A_{\text{flood}} \cdot 10^6$	this study
clay_particle_velocity	m s^{-1}	clay particle velocity	$v_{\text{clay}} = \gamma \cdot \frac{Ar_{\text{clay}}^{\epsilon} \cdot \nu}{\chi \cdot (1 + \gamma \cdot Ar_{\text{clay}}^{\epsilon-1})} \cdot r_{\text{clay}}$	Ahrens 2003
clay_sed_TE	fraction	clay trapping efficiency in lakes and reservoirs	$TE_{\text{clay}} = \frac{RT^3}{l \cdot RT^3 + m \cdot RT^2 - p \cdot RT + t}$	Gill (1979)
	fraction	clay trapping efficiency in coastal ecosystems	$TE_{\text{clay}} = 1 - \exp\left(\frac{-RT}{ST_{\text{clay}}}\right)$	Chen (1975)
clay_time_sed	h	clay particle sedimentation time	$ST_{\text{clay}} = \frac{D_w}{v_{\text{clay}} \cdot 3600}$	-
DBD	g cm^{-3}	dry bulk density in sediments	$DBD = \frac{\alpha}{1 + \alpha \cdot \beta \cdot \%OC_{\text{bur}} \cdot 2}$	Keogh et al. 2021
discharge	m^3 s^{-1}	discharge	$q = runoff \cdot A_{\text{node}} \cdot \frac{10^3}{365 \cdot 24 \cdot 3600}$	-
discharge_max	m^3 s^{-1}	maximum discharge	$q_{\text{max}} = runoff_{\text{max}} \cdot A_{\text{node}} \cdot \frac{10^3}{30 \cdot 24 \cdot 3600}$	-
edge	-	edge flag (1=burial node, 0=not)	edges are nodes which discharge to a NA node, given for the graph using function "out_degree"	this study

https://doi.org/10.5194/egusphere-2025-5359
Preprint. Discussion started: 5 February 2026

Table B2. Model variables – part 2.

Model's variable name	Unit	Description	Calculation/Equation	Reference
frac_clay_expo_local	-	local fraction of clay in the exported sediment that is not deposited, relative to the total non-deposited sediment	$FRAC_{\text{clay-expo-local}} = \frac{SED_{\text{clay-input-total}} - SED_{\text{clay-depo}}}{SED_{\text{input-total}} - SED_{\text{depo}}}$	this study
frac_sand_expo_local	-	local fraction of sand in the exported sediment that is not deposited, relative to the total non-deposited sediment	$FRAC_{\text{sand-expo-local}} = \frac{SED_{\text{sand-input-total}} - SED_{\text{sand-depo}}}{SED_{\text{input-total}} - SED_{\text{depo}}}$	this study
frac_silt_expo_local	-	local fraction of silt in the exported sediment that is not deposited, relative to the total non-deposited sediment	$FRAC_{\text{silt-expo-local}} = \frac{SED_{\text{silt-input-total}} - SED_{\text{silt-depo}}}{SED_{\text{input-total}} - SED_{\text{depo}}}$	this study
frac_clay_input_local	-	local fraction of clay in the imported sediment	$FRAC_{\text{clay-input-local}} = \frac{\text{content}_{\text{clay-input-local}}}{1000}$	Poggio et al. (2021)
frac_sand_input_local	-	local fraction of sand in the imported sediment	$FRAC_{\text{sand-input-local}} = \frac{content_{\text{sand-input-local}}}{1000}$	Poggio et al. (2021)
frac_silt_input_local	-	local fraction of silt in the imported sediment	$FRAC_{\text{silt-input-local}} = \frac{content_{\text{silt-input-local}}}{1000}$	Poggio et al. (2021)
k20	1 d^{-1}	oc mineralization rate at 20ºC	$k_{20} = \kappa \cdot \frac{RT}{24}^{-\eta}$	Catalan et al. 2016
last_coastal	-	burial node flag for coastal ecosystems (1 = burial node, 0 = not)	first coastal ID > 0 and RT > 0 is assigned as a burial node	this study
last_flood	-	burial node flag for floodplains (1 = burial node, 0 = not)	if floodplain ID > 0 and RT > 0 then is a burial node	this study
last_lake	-	burial node flag for lakes (1 = burial node, 0 = not)	if lake ID > 0 and RT > 0 then is a burial node	this study

https://doi.org/10.5194/egusphere-2025-5359
Preprint. Discussion started: 5 February 2026

Table B3. Model variables – part 3.

Model's variable name	Unit	Description	Calculation/Equation	Reference
LSR	cm y^{-1}	linear sedimentation rate	$LSR = \frac{SED_{\mathrm{bur-rate}}}{DBD \cdot 10}$	this study
oc_bur	kg y^{-1}	OC buried (whole-system rate)	$OC_{\mathrm{bur-wc}} = OC_{\mathrm{depo}} \cdot \frac{OCBE}{100}$	this study
oc_bur_rate	g m^{-2} y^{-1}	OC burial (areal rate)	$OC_{\mathrm{bur}} = \frac{OC_{\mathrm{bur-wc}} \cdot 1000}{A_{\mathrm{system}}}$	-
oc_depo	kg y^{-1}	OC deposited into the sediment surface	$OC_{\mathrm{depo}} = SED_{\mathrm{depo}} \cdot \%OC_{\mathrm{depo}}$	-
oc_expo	kg y^{-1}	OC exported to the downstream node	$OC_{\mathrm{expo}} = OC_{\mathrm{input-total}} - OC_{\mathrm{bur}} - OC_{\mathrm{min-total}}$	this study
oc_input_local	kg y^{-1}	local OC input	$OC_{\mathrm{input-local}} = SED_{\mathrm{input-local}} \cdot \frac{\%OC_{\mathrm{input}}}{100}$	Wieder et al. (2014)
oc_input_parents	kg y^{-1}	OC input from parents	sum of OC_{expo} of all parents	this study
oc_input_total	kg y^{-1}	total OC input	$OC_{\mathrm{input-total}} = OC_{\mathrm{input-local}} + OC_{\mathrm{input-parents}}$	this study
oc_min_sed	kg y^{-1}	OC mineralized within the sediments	$OC_{\mathrm{min-sed}} = OC_{\mathrm{depo}} - OC_{\mathrm{bur}}$	this study
oc_min_watercol	kg y^{-1}	OC mineralized in the water column (RT in days)	$OC_{\mathrm{min}} = (OC_{\mathrm{input}} - OC_{\mathrm{depo}}) \cdot (1 - \exp(-k_{20} \cdot \theta^{T_{\mathrm{w}}^{\circ} - 20}) \cdot RT)$	Maavara et al. (2017)
oc_min_total	kg y^{-1}	total mineralized OC	$OC_{\mathrm{min-total}} = OC_{\mathrm{min-sed}} + OC_{\mathrm{min}}$	this study
OCB_eff	%	OC burial efficiency	$OCBE = \frac{100}{1 + \exp(-b \cdot (log(LSR) - c))}$	this study
per_oc_bur	%	percentage of buried OC relative to the total buried sediment	$\%OC_{\mathrm{bur}} = \frac{OC_{\mathrm{bur}}}{SED_{\mathrm{bur}} \cdot 100}$	-
per_oc_depo	%	percentage of deposited OC relative to the total sediment input	$\%OC_{\mathrm{depo}} = \frac{OC_{\mathrm{input-total}} \cdot 100}{SED_{\mathrm{input-total}}}$	this study
R	m	hydraulic radius	$R = \frac{f \cdot q^i \cdot j \cdot q^k}{f \cdot q^i + 2 \cdot j \cdot q^k}$	Schulze et al. (2005)

https://doi.org/10.5194/egusphere-2025-5359
Preprint. Discussion started: 5 February 2026

Table B4. Model variables – part 4.

Model's variable name	Unit	Description	Calculation/Equation	Reference
RT	h	water residence time for lakes, reservoirs, floodplains and coastal ecosystems	$RT = A_{\text{system}} \cdot \frac{D_w}{q \cdot 3600}$	-
	s	water residence time for rivers	$RT = \frac{l}{n \cdot R^{2/3} \cdot s^{1/2}}$	Schulze et al. (2005)
sand_particle_velocity	m s^{-1}	sand particle velocity	$v_{\text{sand}} = \gamma \cdot \frac{Ar_{\text{sand}}^{\epsilon} \cdot \nu}{\chi \cdot (1 + \gamma \cdot Ar_{\text{sand}}^{\epsilon-1})} \cdot r_{\text{sand}}$	Ahrens 2003
sand_sed_TE	fraction	sand trapping efficiency in lakes and reservoirs	$TE_{\text{sand}} = \frac{RT^2}{x \cdot RT^2 + y \cdot RT + z}$	Gill (1979)
	fraction	sand trapping efficiency in coastal ecosystems	$TE_{\text{sand}} = 1 - \exp\left(\frac{-RT}{ST_{\text{sand}}}\right)$	Chen (1975)
sand_time_sed	h	sand particle sedimentation time	$ST_{\text{sand}} = \frac{D_w}{v_{\text{sand}} \cdot 3600}$	-
sed_bur	kg y^{-1}	sediment buried	$SED_{\text{bur}} = SED_{\text{depo}} - OC_{\text{min-sed}}$	this study
sed_bur_rate	kg m^{-2} y^{-1}	sediment burial rate	$SED_{\text{bur-rate}} = \frac{SED_{\text{bur}}}{A_{\text{system}}}$	-
sed_clay_depo	kg y^{-1}	clay portion of the deposited sediments	$SED_{\text{clay-depo}} = SED_{\text{clay-input-total}} \cdot TE_{\text{clay}}$	this study
sed_clay_expo	kg y^{-1}	clay portion of the sediment exported to the downstream node	$SED_{\text{clay-expo}} = SED_{\text{clay-input-total}} - OC_{\text{min}} \cdot FRAC_{\text{clay-expo-local}}$	this study
sed_clay_input_local	kg y^{-1}	clay portion of the local sediment input	$SED_{\text{clay-input-local}} = SED_{\text{input}} \cdot FRAC_{\text{clay-input-local}}$	Borrelli et al. (2017); Poggio et al. (2021)
sed_clay_input_parents	kg y^{-1}	clay portion of the sediment input from parents	sum of $SED_{\text{clay-expo}}$ of all parents	this study
sed_clay_input_total	kg y^{-1}	clay portion of the total sediment input	$SED_{\text{clay-input-total}} = SED_{\text{clay-input-local}} + SED_{\text{clay-input-parents}}$	this study

https://doi.org/10.5194/egusphere-2025-5359
Preprint. Discussion started: 5 February 2026

Table B5. Model variables – part 5.

Model's variable name	Unit	Description	Calculation/Equation	Reference
sed_depo	kg y^{-1}	deposited sediments or net sedimented sediments	$SED_{\text{depo}} = SED_{\text{clay-depo}} + SED_{\text{silt-depo}} + SED_{\text{sand-depo}}$	this study
sed_expo	kg y^{-1}	sediment exported to the downstream node	$SED_{\text{expo}} = SED_{\text{clay-expo}} + SED_{\text{silt-expo}} + SED_{\text{silt-expo}}$	this study
sed_expo_concentration	mg L^{-1}	exported sediment concentration	$SED_{\text{expo-concentration}} = SED_{\text{expo}} \cdot \frac{1000}{q \cdot 365 \cdot 24 \cdot 3600}$	-
sed_input_parents	kg y^{-1}	sediment input from parents	$SED_{\text{input-parents}} = SED_{\text{clay-input-parents}} + SED_{\text{silt-input-parents}} + SED_{\text{sand-input-parents}}$	this study
sed_input_total	kg y^{-1}	total sediment input	$SED_{\text{input-total}} = SED_{\text{input}} + SED_{\text{input-parents}}$	Borrelli et al. (2017)
sed_sand_depo	kg y^{-1}	sand portion of the deposited sediments	$SED_{\text{sand-depo}} = SED_{\text{sed-input-total}} \cdot TE_{\text{sand}}$	this study
sed_sand_expo	kg y^{-1}	sand portion of the sediment exported to the downstream node	$SED_{\text{silt-expo}} = SED_{\text{sed-input-total}} - OC_{\text{min}} \cdot FRAC_{\text{sand-expo-local}}$	this study
sed_sand_input_local	kg y^{-1}	sand portion of the local sediment input	$SED_{\text{silt-expo-local}} = SED_{\text{input}} \cdot FRAC_{\text{sand-input-local}}$	Borrelli et al. (2017); Poggio et al. (2021)
sed_sand_input_parents	kg y^{-1}	sand portion of the sediment input from parents	sum of $SED_{\text{silt-expo}}$ of all parents	this study
sed_sand_input_total	kg y^{-1}	sand portion of the total sediment input	$SED_{\text{sed-input-total}} = SED_{\text{sand-input-local}} + SED_{\text{sand-input-parents}}$	this study
sed_silt_depo	kg y^{-1}	silt portion of the deposited sediments	$SED_{\text{silt-depo}} = SED_{\text{silt-input-total}} \cdot TE_{\text{silt}}$	this study
sed_silt_expo	kg y^{-1}	silt portion of the sediment exported to the donwstream node	$SED_{\text{silt-expo}} = SED_{\text{silt-input-total}} - OC_{\text{min}} \cdot FRAC_{\text{silt-expo-local}}$	this study

https://doi.org/10.5194/egusphere-2025-5359
Preprint. Discussion started: 5 February 2026

https://doi.org/10.5194/egusphere-2025-5359
Preprint. Discussion started: 5 February 2026

Table B6. Model variables – part 6.

Model's variable name	Unit	Description	Calculation/Equation	Reference
sed_silt_input_local	kg y^{-1}	silt portion of the local sediment input	$SED_{\text{silt-input-local}} = SED_{\text{input}} \cdot FRAC_{\text{silt-input-local}}$	Borrelli et al. (2017); Poggio et al. (2021)
sed_silt_input_parents	kg y^{-1}	silt portion of the sediment input from parents	sum of $SED_{\text{silt-expo}}$ of all parents	this study
sed_silt_input_total	kg y^{-1}	silt portion of the total sediment input	$SED_{\text{silt-input-total}} = SED_{\text{silt-input-local}} + SED_{\text{silt-input-parents}}$	this study
silt_particle_velocity	m s^{-1}	silt particle velocity	$v_{\text{silt}} = \gamma \cdot \frac{Ar_{\text{silt}}^{\epsilon} \cdot \nu}{\chi \cdot (1 + \gamma \cdot Ar_{\text{silt}}^{\epsilon-1})} \cdot r_{silt}$	Ahrens 2003
silt_sed_TE	fraction	silt trapping efficiency in lakes and reservoirs	$TE_{\text{silt}} = \frac{RT}{u + w \cdot RT}$	Gill (1979)
	fraction	silt trapping efficiency in coastal ecosystems	$TE_{\text{silt}} = 1 - \exp\left(\frac{-RT}{ST_{\text{silt}}}\right)$	Chen (1975)
silt_time_sed	h	silt particle sedimentation time	$ST_{\text{silt}} = \frac{D_w}{v_{\text{silt}} \cdot 3600}$	-
water_depth	m	water depth for rivers	$D_w = d \cdot q^e$	-

https://doi.org/10.5194/egusphere-2025-5359
Preprint. Discussion started: 5 February 2026

Table B7. Model parameters -part 1.

Model's parameter name	Symbol	Value	Unit	Description	Reference
a_dbd	α	2.296	-	dry bulk density coefficient	Keogh et al. (2021)
b_dbd	β	0.139	-	dry bulk density coefficient	Keogh et al. (2021)
b_sigm	b	0.7068	-	parameter of the LSR vs OCBE relationship	this study
c_sigm	c	-0.78	-	parameter of the LSR vs OCBE relationship (-1.84 for coastal systems)	this study
clay_radius	r_{clay}	0.1E-05	m	clay particle radius	Hatono and Yoshimura (2020)
d	d	0.27	-	water depth coefficient	Andreadis et al. (2013)
density_clay_particle	δ_{clay}	1800	kg/m^3	clay particle density	this study
density_fluid	δ_w	998	kg/m^3	average water density	this study
density_silt_particle	δ_{silt}	1700	kg/m^3	silt particle density	this study
density_sand_particle	δ_{sand}	1600	kg/m^3	sand particle density	this study
e	e	0.3	-	water depth coefficient	Andreadis et al. (2013)
f	f	2.71	-	hydraulic radius coefficient	Schulze et al. (2005)
g	g	9.8	m/s^2	gravitational acceleration	this study
i	i	0.557	-	hydraulic radius coefficient	Schulze et al. (2005)
j	j	0.349	-	hydraulic radius coefficient	Schulze et al. (2005)
k	k	0.341	-	hydraulic radius coefficient	Schulze et al. (2005)
mu	μ	0.001	kg m^{-1} s^{-1}	dynamic viscosity	this study
n	n	0.044	s m$^{1/3}$	Manning coefficient	Font et al. (2019)
nu	ν	1.002E-06	m^2 s^{-1}	kinematic viscosity: μ/δ_w	this study

https://doi.org/10.5194/egusphere-2025-5359
Preprint. Discussion started: 5 February 2026

Table B8. Model parameters -part 2.

Model's parameter name	Symbol	Value	Unit	Description	Reference
param_theta	θ	1.07	-	temperature correction coefficient	Maavara et al. (2017)
param_gamma	γ	24.6	-	fall velocity coefficient	Ahrens (2003)
param_epsilon	ϵ	0.477	-	fall velocity coefficient	Ahrens (2003)
param_chi	χ	17.9	-	fall velocity coefficient	Ahrens (2003)
param_kappa	κ	0.0147	-	decay rate coefficient	Catalán et al. (2016)
param_eta	η	-0.448	-	decay rate coefficient	Catalán et al. (2016)
sand_radius	r_{sand}	0.001	m	sand particle radius	Hatono and Yoshimura (2020)
silt_radius	r_{silt}	0.25E-04	m	silt particle radius	Hatono and Yoshimura (2020)
TE_l	l	1.02655	-	clay trapping efficiency coefficient	Gill (1979)
TE_m	m	0.02621	-	clay trapping efficiency coefficient	Gill (1979)
TE_p	p	0.133E-03	-	clay trapping efficiency coefficient	Gill (1979)
TE_t	t	0.1E-05	-	clay trapping efficiency coefficient	Gill (1979)
TE_u	u	0.012	-	silt trapping efficiency coefficient	Gill (1979)
TE_w	w	1.02	-	silt trapping efficiency coefficient	Gill (1979)
TE_x	x	0.994701	-	sand trapping efficiency coefficient	Gill (1979)
TE_y	y	0.006297	-	sand trapping efficiency coefficient	Gill (1979)
TE_z	z	0.3E-05	-	sand trapping efficiency coefficient	Gill (1979)

https://doi.org/10.5194/egusphere-2025-5359
Preprint. Discussion started: 5 February 2026

Author contributions. **DH:** conceptualization, methodology, model development, coding, data curation and processing, model output analysis and validation validation, writing - original draft, visualization; **NC:** conceptualization, methodology, model output analysis, writing - review & editing, supervision; **BO:** conceptualization, writing - review & editing, supervision, funding acquisition; **RM:** conceptualization, methodology, model development, coding, model output analysis and validation, writing - review & editing, supervision, funding acquisition.

Competing interests. The authors declare no conflict of interest.

Acknowledgements. This project has received funding from the European Union's Horizon 2020 research and innovation programme under the Marie Skłodowska-Curie grant agreement No. 956623. RM and BO acknowledge support from projects PID2024-161534NB-C31 and PID2024-161534NB-C33, funded by MCIN/AEI/10.13039/501100011033/. NC's research was funded by project PID2022-140848NA-C32 of the Spanish MCIN /AEI. We thank Janick Klink for providing the original code and for his valuable support during the initial coding phase. We are also grateful to to Lluís Bosch for his assistance using the cluster, and to Daniel Mercado for his guidance on data sources and processing, as well as for his constructive reviewing comments. Finally, we thank Aurora Martinez, Oscar Serrano and Jordi Pagès for their insightful feedback on the conceptualization of coastal ecosystem components.

https://doi.org/10.5194/egusphere-2025-5359
Preprint. Discussion started: 5 February 2026

References

Ahrens, J. P.: Simple Equations to Calculate Fall Velocity and Sediment Scale Parameter, Journal of Waterway, Port, Coastal, and Ocean Engineering, 129, 146–150, https://doi.org/10.1061/(asce)0733-950x(2003)129:3(146), 2003.

Anderson, N. J., Bennion, H., and Lotter, A. F.: Lake eutrophication and its implications for organic carbon sequestration in Europe, Global Change Biology, 20, 2741–2751, https://doi.org/10.1111/gcb.12584, 2014.

Andreadis, K. M., Schumann, G. J., and Pavelsky, T.: A simple global river bankfull width and depth database, Water Resources Research, 49, 7164–7168, https://doi.org/10.1002/wrcr.20440, 2013.

Aufdenkampe, A. K., Mayorga, E., Raymond, P. A., Melack, J. M., Doney, S. C., Alin, S. R., Aalto, R. E., and Yoo, K.: Riverine coupling of biogeochemical cycles between land, oceans, and atmosphere, Frontiers in Ecology and the Environment, 9, 53–60, https://doi.org/10.1890/100014, 2011.

Battin, T. J., Luyssaert, S., Kaplan, L. A., Aufdenkampe, A. K., Richter, A., and Tranvik, L. J.: The boundless carbon cycle, Nature Geoscience, 2, 598–600, https://doi.org/10.1038/ngeo618, 2009.

Bernal, B. and Mitsch, W. J.: Carbon sequestration in freshwater wetlands in Costa Rica and Botswana, Biogeochemistry, 115, 77–93, https://doi.org/10.1007/s10533-012-9819-8, 2013.

Betts, J. N. and Holland, H. D.: The oxygen content of ocean bottom waters, the burial efficiency of organic carbon, and the regulation of atmospheric oxygen, Palaeogeography, Palaeoclimatology, Palaeoecology, 97, 5–18, https://doi.org/10.1016/0031-0182(91)90178-T, 1991.

Beusen, A. H., Dekkers, A. L., Bouwman, A. F., Ludwig, W., and Harrison, J.: Estimation of global river transport of sediments and associated particulate C, N, and P, Global Biogeochemical Cycles, 19, https://doi.org/10.1029/2005GB002453, 2005.

Borrelli, P., Robinson, D. A., Fleischer, L. R., Lugato, E., Ballabio, C., Alewell, C., Meusburger, K., Modugno, S., Schütt, B., Ferro, V., et al.: An assessment of the global impact of 21st century land use change on soil erosion, Nature communications, 8, 2013, 2017.

Breithaupt, J. L., Smoak, J. M., Smith III, T. J., Sanders, C. J., and Hoare, A.: Organic carbon burial rates in mangrove sediments: Strengthening the global budget, GLOBAL BIOGEOCHEMICAL CYCLES, 26, https://doi.org/10.1029/2012GB004375, 2012.

Brune, G. M.: Trap efficiency of reservoirs, Eos, Transactions American Geophysical Union, 34, 407–418, 1953.

Catalán, N., Marcé, R., Kothawala, D. N., and Tranvik, L. J.: Organic carbon decomposition rates controlled by water retention time across inland waters, Nature Geoscience, 9, 501–504, https://doi.org/10.1038/ngeo2720, 2016.

Chen, C.-N.: Design of sediment retention basins, in: Proceedings of the National Symposium on Urban Hydrology and Sediment Control, July 28-31, 1975., UKY BU109, 1975.

Dethier, E. N., Renshaw, C. E., and Magilligan, F. J.: Rapid changes to global river suspended sediment flux by humans, Science, 376, 1447–1452, https://doi.org/10.1126/science.abn7980, 2022.

Dietz, R. D., Engstrom, D. R., and Anderson, N. J.: Patterns and drivers of change in organic carbon burial across a diverse landscape: Insights from 116 Minnesota lakes, Global Biogeochemical Cycles, 29, 708–727, https://doi.org/10.1002/2014GB004952, 2015.

Drake, T. W., Raymond, P. A., and Spencer, R. G.: Terrestrial carbon inputs to inland waters: A current synthesis of estimates and uncertainty, Limnology And Oceanography Letters, 3, 132–142, https://doi.org/10.1002/lol2.10055, 2018.

Druon, J. N., Mannino, A., Signorini, S., McClain, C., Friedrichs, M., Wilkin, J., and Fennel, K.: Modeling the dynamics and export of dissolved organic matter in the Northeastern U.S. continental shelf, Estuarine, Coastal and Shelf Science, 88, 488–507, https://doi.org/10.1016/j.ecss.2010.05.010, 2010.

https://doi.org/10.5194/egusphere-2025-5359
Preprint. Discussion started: 5 February 2026

Duarte, C. M., Losada, I. J., Hendriks, I. E., Mazarrasa, I., and Marbà, N.: The role of coastal plant communities for climate change mitigation and adaptation, Nature Climate Change, 3, 961–968, https://doi.org/10.1038/nclimate1970, 2013.

Fekete, B. M., Vörösmarty, C. J., and Grabs, W.: High-resolution fields of global runoff combining observed river discharge and simulated water balances, Global Biogeochemical Cycles, 16, 15–1–15–10, https://doi.org/10.1029/1999gb001254, 2002.

Ferland, M.-E., Prairie, Y. T., Teodoru, C., and del Giorgio, P. A.: Linking organic carbon sedimentation, burial efficiency, and long-term accumulation in boreal lakes, Journal of Geophysical Research: Biogeosciences, 119, 836–847, https://doi.org/10.1002/2013JG002345, 2014.

Font, C., Bregoli, F., Acuña, V., Sabater, S., and Marcé, R.: GLOBAL-FATE: A GIS-based model for assessing contaminants fate in the global river network, Geoscientific Model Development, 12, 5213–5228, https://doi.org/10.5194/gmd-2019-8, 2019.

Friedlingstein, P., Jones, M. W., O'Sullivan, M., Andrew, R. M., and Bakker, D. C.: Global Carbon Budget 2021, raport Earth System Science Data, Earth System Science Data, 14, 1917–2005, 2022.

Futter, M. N., Butterfield, D., Cosby, B. J., Dillon, P. J., Wade, A. J., and Whitehead, P. G.: Modeling the mechanisms that control in-stream dissolved organic carbon dynamics in upland and forested catchments, Water Resources Research, 43, 1–16, https://doi.org/10.1029/2006WR004960, 2007.

Galy, V., Peucker-Ehrenbrink, B., and Eglinton, T.: Global carbon export from the terrestrial biosphere controlled by erosion, Nature, 521, 204–207, https://doi.org/10.1038/nature14400, 2015.

Geyman, E. C., Ke, Y., Magyar, J. S., Reahl, J. N., Soldano, V., Brown, N. D., West, A. J., Fischer, W. W., and Lamb, M. P.: Scaling laws for sediment storage and turnover in river floodplains, Science Advances, 11, 1–13, https://doi.org/10.1126/sciadv.adu8574, 2025.

Gill, M. A.: Sedimentation and useful life of reservoirs, Journal of Hydrology, 44, 89–95, 1979.

Golub, M., Thiery, W., Marcé, R., Pierson, D., Vanderkelen, I., Mercado-Bettin, D., Woolway, R. I., Grant, L., Jennings, E., Kraemer, B. M., Schewe, J., Zhao, F., Frieler, K., Mengel, M., Bogomolov, V. Y., Bouffard, D., Côté, M., Couture, R. M., Debolskiy, A. V., Droppers, B., Gal, G., Guo, M., Janssen, A. B., Kirillin, G., Ladwig, R., Magee, M., Moore, T., Perroud, M., Piccolroaz, S., Raaman Vinnaa, L., Schmid, M., Shatwell, T., Stepanenko, V. M., Tan, Z., Woodward, B., Yao, H., Adrian, R., Allan, M., Anneville, O., Arvola, L., Atkins, K., Boegman, L., Carey, C., Christianson, K., De Eyto, E., Degasperi, C., Grechushnikova, M., Hejzlar, J., Joehnk, K., Jones, I. D., Laas, A., MacKay, E. B., Mammarella, I., Markensten, H., McBride, C., Özkundakci, D., Potes, M., Rinke, K., Robertson, D., Rusak, J. A., Salgado, R., Van Der Linden, L., Verburg, P., Wain, D., Ward, N. K., Wollrab, S., and Zdorovennova, G.: A framework for ensemble modelling of climate change impacts on lakes worldwide: The ISIMIP Lake Sector, Geoscientific Model Development, 15, 4597–4623, https://doi.org/10.5194/gmd-15-4597-2022, 2022.

Gommet, C., Lauerwald, R., Ciais, P., Guenet, B., Zhang, H., and Regnier, P.: Spatiotemporal patterns and drivers of terrestrial dissolved organic carbon (DOC) leaching into the European river network, Earth System Dynamics, 13, 393–418, https://doi.org/10.5194/esd-13-393-2022, 2022.

Gosling, S., Müller Schmied, H., Betts, R., Chang, J., Ciais, P., Dankers, R., Döll, P., Eisner, S., Flörke, M., Gerten, D., et al.: ISIMIP2a simulation data from water (global) sector (V. 1.1), ISIMIP2a Simulation Data from Water (global) Sector (V. 1.1), 2019.

Gosling, S. N., Schmied, H. M., Bradley, A., Burek, P., Chang, J., Ciais, P., Grillakis, M., Guillaumot, L., Hanasaki, N., Hartley, A., Huang, H., Kou-Giesbrecht, S., Koutroulis, A., Ostberg, S., Otta, K., Qi, W., Satoh, Y., Stacke, T., Zhu, Q., and Schewe, J.: ISIMIP3a Simulation Data from the Global Water Sector, https://doi.org/10.48364/ISIMIP.398165.5, 2025.

Greenberg, E., Chadwick, A. J., Li, G. K., and Ganti, V.: Quantifying Channel Mobility and Floodplain Reworking Timescales Across River Planform Morphologies, Geophysical Research Letters, 51, https://doi.org/10.1029/2024GL108537, 2024.

https://doi.org/10.5194/egusphere-2025-5359
Preprint. Discussion started: 5 February 2026

Gudasz, C., Ruppenthal, M., Kalbitz, K., Cerli, C., Fiedler, S., Oelmann, Y., Andersson, A., and Karlsson, J.: Contributions of terrestrial organic carbon to northern lake sediments, Limnology And Oceanography Letters, 2, 218–227, https://doi.org/10.1002/lol2.10051, 2017.

Guillemette, F., McCallister, S. L., and del Giorgio, P. A.: Differentiating the degradation dynamics of algal and terrestrial carbon within complex natural dissolved organic carbon in temperate lakes, Journal of Geophysical Research: Biogeosciences, 118, 963–973, 2013.

Hagberg, A. A., Schult, D. A., and Swart, P. J.: Exploring network structure, dynamics, and function using NetworkX, in: Proceedings of the 7th Python in Science Conference (SciPy 2008), pp. 11–15, 2008.

Hanson, P. C., Buffam, I., Rusak, J. A., Stanley, E. H., and Watras, C.: Quantifying lake allochthonous organic carbon budgets using a simple equilibrium model, Limnology and Oceanography, 59, 167–181, https://doi.org/10.4319/lo.2014.59.1.0167, 2014.

Hatono, M. and Yoshimura, K.: Development of a global sediment dynamics model, Progress in Earth and Planetary Science, 7, https://doi.org/10.1186/s40645-020-00368-6, 2020.

Heathcote, A. J., Anderson, N. J., Prairie, Y. T., Engstrom, D. R., and Del Giorgio, P. A.: Large increases in carbon burial in northern lakes during the Anthropocene, Nature Communications, 6, 1–6, https://doi.org/10.1038/ncomms10016, 2015.

Henry, D.: Code, Input and Output files LOAC-OCB model [Data set], Zenodo, https://doi.org/10.5281/zenodo.17476679, 2025.

Henry, D., Catalán, N., Obrador, B., and Marcé, R.: Modeling carbon burial along the land to ocean aquatic continuum: Current status, challenges and perspectives, Earth-Science Reviews, 253, 104 791, https://doi.org/10.1016/j.earscirev.2024.104791, 2024.

Hoffmann, T., Schlummer, M., Notebaert, B., Verstraeten, G., and Korup, O.: Carbon burial in soil sediments from Holocene agricultural erosion, Central Europe, Global Biogeochemical Cycles, 27, 828–835, https://doi.org/10.1002/gbc.20071, 2013.

Ingall, E. D. and Cappellen, P. V.: Relation between sedimentation rate and burial of organic phosphorus and organic carbon in marine sediments, Geochimica et Cosmochimica Acta, 54, 373–386, https://doi.org/10.1016/0016-7037(90)90326-G, 1990.

Katsev, S. and Crowe, S. A.: Organic carbon burial efficiencies in sediments: The power law of mineralization revisited, Geology, 43, 607–610, https://doi.org/10.1130/G36626.1, 2015.

Keogh, M. E., Törnqvist, T. E., Kolker, A. S., Erkens, G., and Bridgeman, J. G.: Organic Matter Accretion, Shallow Subsidence, and River Delta Sustainability, Journal of Geophysical Research: Earth Surface, 126, 1–21, https://doi.org/10.1029/2021JF006231, 2021.

Kirwan, M. L., Megonigal, J. P., Noyce, G. L., and Smith, A. J.: Geomorphic and ecological constraints on the coastal carbon sink, Nature Reviews Earth and Environment, 4, 393–406, https://doi.org/10.1038/s43017-023-00429-6, 2023.

Klink, J., Perelló, L. A., Abily, M., Saló, J., Rodríguez-Roda, I., Marcé, R., Gernjak, W., and Corominas, L.: Coupling hydrological and sanitation datasets to simulate wastewater-derived contamination in European rivers: Model development and calibration, Environmental Modelling & Software, 178, 106 049, 2024.

Kortelainen, P., Rantakari, M., Pajunen, H., Mattsson, T., Juutinen, S., Larmola, T., Alm, J., Silvola, J., and Martikainen, P. J.: Carbon evasion/accumulation ratio in boreal lakes is linked to nitrogen, Global Biogeochemical Cycles, 27, 363–374, https://doi.org/10.1002/gbc.20036, 2013.

Kothawala, D. N., Kellerman, A. M., Catalán, N., and Tranvik, L. J.: Organic Matter Degradation across Ecosystem Boundaries: The Need for a Unified Conceptualization, Trends in Ecology and Evolution, 36, 113–122, https://doi.org/10.1016/j.tree.2020.10.006, 2021.

Kunz, M. J., Anselmetti, F. S., West, A., Wehrli, B., Vollenweider, A., Thüring, S., and Senn, D. B.: Sediment accumulation and carbon, nitrogen, and phosphorus deposition in the large tropical reservoir Lake Kariba (Zambia/Zimbabwe), Journal of Geophysical Research: Biogeosciences, 116, 1–13, https://doi.org/10.1029/2010JG001538, 2011.

Lal, R.: Soil erosion and the global carbon budget, Environment International, 29, 437–450, https://doi.org/10.1016/S0160-4120(02)00192-7, 2003.

https://doi.org/10.5194/egusphere-2025-5359
Preprint. Discussion started: 5 February 2026

Lehner, B. and Döll, P.: Development and validation of a global database of lakes, reservoirs and wetlands, Journal of hydrology, 296, 1–22, 2004.

Lehner, B. and Grill, G.: Global river hydrography and network routing: baseline data and new approaches to study the world's large river systems, Hydrological Processes, 27, 2171–2186, 2013.

Lehner, B., Verdin, K., and Jarvis, A.: New global hydrography derived from spaceborne elevation data, Eos, Transactions American Geophysical Union, 89, 93–94, 2008.

Lehner, B., Anand, M., Fluet-Chouinard, E., Tan, F., Aires, F., Allen, G. H., Bousquet, P., Canadell, J. G., Davidson, N., Ding, M., et al.: Mapping the world's inland surface waters: an upgrade to the Global Lakes and Wetlands Database (GLWD v2), Earth System Science Data, 17, 2277–2329, 2025.

Leopold, L. B. and Maddock, T.: The hydraulic geometry of stream channels and some physiographic implications, vol. 252, US Government Printing Office, 1953.

Li, J., Crowe, S. A., Miklesh, D., Kistner, M., Canfield, D. E., and Katsev, S.: Carbon mineralization and oxygen dynamics in sediments with deep oxygen penetration, Lake Superior, Limnology and Oceanography, 57, 1634–1650, https://doi.org/10.4319/lo.2012.57.6.1634, 2012.

Li, M., Peng, C., and He, N.: Global patterns of particulate organic carbon export from land to the ocean, Ecohydrology, 15, https://doi.org/10.1002/eco.2373, 2022.

Li, S., Li, H., Tang, T., and Wang, S.: The Ballast Effect of Terrigenous Lithogenic Particles From Rivers and Its Influence on POC Fluxes in the Ocean, Global Biogeochemical Cycles, 38, 1–21, https://doi.org/10.1029/2024GB008155, 2024.

Lininger, K. B. and Wohl, E.: Floodplain dynamics in North American permafrost regions under a warming climate and implications for organic carbon stocks: A review and synthesis, Earth-Science Reviews, 193, 24–44, https://doi.org/10.1016/j.earscirev.2019.02.024, 2019.

Liu, M., Raymond, P. A., Lauerwald, R., Zhang, Q., Trapp-Müller, G., Davis, K. L., Moosdorf, N., Xiao, C., Middelburg, J. J., Bouwman, A. F., Beusen, A. H., Peng, C., Lacroix, F., Tian, H., Wang, J., Li, M., Zhu, Q., Cohen, S., van Hoek, W. J., Li, Y., Li, Y., Yao, Y., and Regnier, P.: Global riverine land-to-ocean carbon export constrained by observations and multi-model assessment, Nature Geoscience, 17, 896–904, https://doi.org/10.1038/s41561-024-01524-z, 2024.

Lovelock, C. E. and Reef, R.: Variable Impacts of Climate Change on Blue Carbon, One Earth, 3, 195–211, https://doi.org/10.1016/j.oneear.2020.07.010, 2020.

Luhar, M., Infantes, E., Orfila, A., Terrados, J., and Nepf, H. M.: Field observations of wave-induced streaming through a submerged seagrass (Posidonia oceanica) meadow, Journal of Geophysical Research: Oceans, 118, 1955–1968, 2013.

Luo, Z., Ma, J. M., Zheng, S. L., Nan, C. Z., and Nie, L. M.: Different hydrodynamic conditions on the deposition of organic carbon in sediment of two reservoirs, Hydrobiologia, 765, 15–26, https://doi.org/10.1007/s10750-015-2410-2, 2016.

Maavara, T., Lauerwald, R., Regnier, P., and Van Cappellen, P.: Global perturbation of organic carbon cycling by river damming, Nature Communications, 8, 15 347, https://doi.org/10.1038/ncomms15347, 2017.

Marcé, R., Obrador, B., Morguí, J.-A., Lluís Riera, J., López, P., and Armengol, J.: Carbonate weathering as a driver of CO2 supersaturation in lakes, Nature Geoscience, 8, 107–111, 2015.

Mayorga, E., Seitzinger, S. P., Harrison, J. A., Dumont, E., Beusen, A. H., Bouwman, A. F., Fekete, B. M., Kroeze, C., and Van Drecht, G.: Global Nutrient Export from WaterSheds 2 (NEWS 2): Model development and implementation, Environmental Modelling and Software, 25, 837–853, https://doi.org/10.1016/j.envsoft.2010.01.007, 2010.

https://doi.org/10.5194/egusphere-2025-5359
Preprint. Discussion started: 5 February 2026

Mcowen, C. J., Weatherdon, L. V., Van Bochove, J.-W., Sullivan, E., Blyth, S., Zockler, C., Stanwell-Smith, D., Kingston, N., Martin, C. S., Spalding, M., et al.: A global map of saltmarshes, Biodiversity Data Journal, p. e11764, https://doi.org/doi.org/10.3897/BDJ.5.e11764, 2017.

Mendonça, R., Kosten, S., Sobek, S., Cardoso, S. J., Figueiredo-Barros, M. P., Estrada, C. H. D., and Roland, F.: Organic carbon burial efficiency in a subtropical hydroelectric reservoir, Biogeosciences, 13, 3331–3342, https://doi.org/10.5194/bg-13-3331-2016, 2016.

Mendonça, R., Müller, R. A., Clow, D., Verpoorter, C., Raymond, P., Tranvik, L. J., and Sobek, S.: Organic carbon burial in global lakes and reservoirs, Nature Communications, 8, 1694, https://doi.org/10.1038/s41467-017-01789-6, 2017.

Messager, M. L., Lehner, B., Grill, G., Nedeva, I., and Schmitt, O.: Estimating the volume and age of water stored in global lakes using a geo-statistical approach, Nature communications, 7, 1–11, 2016.

Moreira-Turcq, P., Jouanneau, J. M., Turcq, B., Seyler, P., Weber, O., and Guyot, J. L.: Carbon sedimentation at Lago Grande de Curuai, a floodplain lake in the low Amazon region: Insights into sedimentation rates, Palaeogeography, Palaeoclimatology, Palaeoecology, 214, 27–40, https://doi.org/10.1016/j.palaeo.2004.06.013, 2004.

Mulholland, P. J. and Elwood, J. W.: The role of lake and reservoir sediments as sinks in the perturbed global carbon cycle., Tellus, 34, 490–499, https://doi.org/10.3402/tellusa.v34i5.10834, 1982.

Noe, G. B. and Hupp, C. R.: Retention of riverine sediment and nutrient loads by coastal plain floodplains, Ecosystems, 12, 728–746, https://doi.org/10.1007/s10021-009-9253-5, 2009.

O'Callaghan, J. F. and Mark, D. M.: The extraction of drainage networks from digital elevation data, Computer vision, graphics, and image processing, 28, 323–344, 1984.

Ouyang, X. and Lee, S. Y.: Updated estimates of carbon accumulation rates in coastal marsh sediments, Biogeosciences, 11, 5057–5071, https://doi.org/10.5194/bg-11-5057-2014, 2014.

Pittman, B., Jones, J. R., Millspaugh, J. J., Kremer, R. J., and Downing, J. A.: Sediment organic carbon distribution in 4 small northern missouri impoundments: Implications for sampling and carbon sequestration, Inland Waters, 3, 39–46, https://doi.org/10.5268/IW-3.1.507, 2013.

Poggio, L., De Sousa, L. M., Batjes, N. H., Heuvelink, G. B., Kempen, B., Ribeiro, E., and Rossiter, D.: SoilGrids 2.0: producing soil information for the globe with quantified spatial uncertainty, Soil, 7, 217–240, 2021.

Regnier, P., Resplandy, L., Najjar, R. G., and Ciais, P.: The land-to-ocean loops of the global carbon cycle, Nature, 603, 401–410, https://doi.org/10.1038/s41586-021-04339-9, 2022.

Ricker, M. C. and Lockaby, B. G.: Soil Organic Carbon Stocks in a Large Eutrophic Floodplain Forest of the Southeastern Atlantic Coastal Plain, USA, Wetlands, 35, 291–301, https://doi.org/10.1007/s13157-014-0618-y, 2015.

Rosentreter, J. A., Laruelle, G. G., Bange, H. W., Bianchi, T. S., Busecke, J. J., Cai, W. J., Eyre, B. D., Forbrich, I., Kwon, E. Y., Maavara, T., Moosdorf, N., Najjar, R. G., Sarma, V. V., Van Dam, B., and Regnier, P.: Coastal vegetation and estuaries are collectively a greenhouse gas sink, Nature Climate Change, 13, 579–587, https://doi.org/10.1038/s41558-023-01682-9, 2023.

Rouault, E., Warmerdam, F., Schwehr, K., Kiselev, A., Butler, H., Łoskot, M., Szekeres, T., Tourigny, E., Landa, M., Miara, I., et al.: Gdal, Zenodo, https://doi.org/10.5281/zenodo.15869424, 2023.

Sanders, L. M., Taffs, K. H., Stokes, D. J., Sanders, C. J., Smoak, J. M., Enrich-Prast, A., Macklin, P. A., Santos, I. R., and Marotta, H.: Carbon accumulation in Amazonian floodplain lakes: A significant component of Amazon budgets?, Limnology And Oceanography Letters, 2, 29–35, https://doi.org/10.1002/lol2.10034, 2017.

https://doi.org/10.5194/egusphere-2025-5359
Preprint. Discussion started: 5 February 2026

Schlünz, B. and Schneider, R. R.: Transport of terrestrial organic carbon to the oceans by rivers: Re-estimating flux- and burial rates, International Journal of Earth Sciences, 88, 599–606, https://doi.org/10.1007/s005310050290, 2000.

Schulze, K., Hunger, M., and Döll, P.: Simulating river flow velocity on global scale, Advances in Geosciences, 5, 133–136, 2005.

Serrano, O., Lavery, P. S., López-Merino, L., Ballesteros, E., and Mateo, M. A.: Location and associated carbon storage of erosional escarpments of seagrass Posidonia mats, Frontiers in Marine Science, 3, 1–7, https://doi.org/10.3389/fmars.2016.00042, 2016.

Short, F.: UNEP-WCMC. Global distribution of seagrasses (version 7.1). Seventh update to the data layer used in Green and Short (2003), superseding version 6. Cambridge (UK): UN Environment World Conservation Monitoring Centre, 2020.

Siikamäki, J., Sanchirico, J. N., Jardine, S., McLaughlin, D., and Morris, D.: Blue carbon: Coastal ecosystems, their carbon storage, and potential for reducing emissions, Environment, 55, 14–29, https://doi.org/10.1080/00139157.2013.843981, 2013.

Sikder, M. S., Wang, J., Allen, G. H., Sheng, Y., Yamazaki, D., Song, C., Ding, M., Crétaux, J. F., and Pavelsky, T. M.: Lake-TopoCat: a global lake drainage topology and catchment database, Earth System Science Data, 15, 3483–3511, https://doi.org/10.5194/essd-15-3483-2023, 2023.

Sobek, S., Durisch-Kaiser, E., Zurbrug¨g, R., Wongfun, N., Wessels, M., Pasche, N., and Wehrli, B.: Organic carbon burial efficiency in lake sediments controlled by oxygen exposure time and sediment source, Limnology and Oceanography, 54, 2243–2254, https://doi.org/10.4319/lo.2009.54.6.2243, 2009.

Sobek, S., Zurbrügg, R., and Ostrovsky, I.: The burial efficiency of organic carbon in the sediments of Lake Kinneret, Aquatic Sciences, 73, 355–364, https://doi.org/10.1007/s00027-011-0183-x, 2011.

Sobek, S., Delsontro, T., Wongfun, N., and Wehrli, B.: Extreme organic carbon burial fuels intense methane bubbling in a temperate reservoir, Geophysical Research Letters, 39, 2–5, https://doi.org/10.1029/2011GL050144, 2012.

Sobek, S., Anderson, N. J., Bernasconi, S. M., and Del Sontro, T.: Low organic carbon burial efficiency in arctic lake sediments, Journal of Geophysical Research: Biogeosciences, 119, 1231–1243, https://doi.org/10.1002/2014JG002612, 2014.

Spalding, M., Kainuma, M., and Collins, L.: World atlas of mangroves. A collaborative project of ITTO, ISME, FAO, UNEP-WCMC, UNESCO-MAB, UNU-INWEH and TNC. London (UK): Earthscan, London, Routledge, 2010.

Tamooh, F., Van Den Meersche, K., Meysman, F., Marwick, T. R., Borges, A. V., Merckx, R., Dehairs, F., Schmidt, S., Nyunja, J., and Bouillon, S.: Distribution and origin of suspended matter and organic carbon pools in the Tana River Basin, Kenya, Biogeosciences, 9, 2905–2920, https://doi.org/10.5194/bg-9-2905-2012, 2012.

Tian, H., Yang, Q., Najjar, R. G., Ren, W., Friedrichs, M. A. M., Hopkinson, C. S., and Pan, S.: Anthropogenic and climatic influences on carbon fluxes from eastern North America to the Atlantic Ocean: A process-based modeling study, Journal of Geophysical Research: Biogeosciences, 120, 757–772, https://doi.org/10.1002/2014JG002760, 2015.

Torres, M. A., Limaye, A. B., Ganti, V., Lamb, M. P., Joshua West, A., and Fischer, W. W.: Model predictions of long-lived storage of organic carbon in river deposits, Earth Surface Dynamics, 5, 711–730, https://doi.org/10.5194/esurf-5-711-2017, 2017.

Tranvik, L. J., Downing, J. A., Cotner, J. B., Loiselle, S. A., Striegl, R. G., Ballatore, T. J., ..., and Weyhenmeyer, G. A.: Lakes and reservoirs as regulators of carbon cycling and climate, Limnology and Oceanography, 54, 2298–2314, 2009.

Twilley, R. R., Chen, R. H., and Hargis, T.: Carbon sinks in mangroves and their implications to carbon budget of tropical coastal ecosystems, Water, Air, & Soil Pollution, 64, 265–288, https://doi.org/10.1007/BF00477106, 1992.

VERDIN, K.: ISLSCP II HYDRO1k Elevation-derived Products, https://doi.org/10.3334/ORNLDAAC/1007, 2011.

Walling, D. E., Fang, D., Nicholas, A. P., and Sweet, R. J.: River flood plains as carbon sinks, IAHS-AISH Publication, pp. 460–470, 2006.

https://doi.org/10.5194/egusphere-2025-5359
Preprint. Discussion started: 5 February 2026

Webb, J. R., Santos, I. R., Maher, D. T., and Finlay, K.: The Importance of Aquatic Carbon Fluxes in Net Ecosystem Carbon Budgets: A Catchment-Scale Review, Ecosystems, 22, 508–527, https://doi.org/10.1007/s10021-018-0284-7, 2019.

Wieder, W., Boehnert, J., Bonan, G., and Langseth, M.: Regridded harmonized world soil database v1. 2, Ornl Daac, https://doi.org/10.3334/ORNLDAAC/1247, 2014.

780 Wu, H., Kimball, J. S., Li, H., Huang, M., Leung, L. R., and Adler, R. F.: A new global river network database for macroscale hydrologic modeling, Water resources research, 48, 2012.

Yang, S., Shi, B., Bouma, T., Ysebaert, T., and Luo, X.: Wave attenuation at a salt marsh margin: a case study of an exposed coast on the Yangtze Estuary, Estuaries and Coasts, 35, 169–182, 2012.

Zhang, P. and Chartrand, G.: Introduction to graph theory, vol. 2, Tata McGraw-Hill New York, 2006.